

# Interfacial electrohydrodynamic solitary waves under horizontal electric fields

Xin Guan<sup>1,2</sup> and Zhan Wang<sup>1,3,†</sup>

<sup>1</sup>Institute of Mechanics, Chinese Academy of Sciences, Beijing 100190, PR China

<sup>2</sup>Department of Mathematics, University College London, London WC1E 6BT, UK

<sup>3</sup>University of Chinese Academy of Sciences, Beijing 100049, PR China

(Received 25 September 2021; revised 6 March 2022; accepted 14 March 2022)

Interfacial waves between two superimposed dielectric fluid layers under a horizontal electric field are investigated from asymptotic and numerical aspects. The fluid is taken to be inviscid, incompressible and non-conducting in each layer. The competing forces resulting from gravity, surface tension and electric field are all considered. A systematic procedure is proposed to derive model equations of multiple scales in various possible limits from the electrified Euler equations in the framework of the Zakharov–Craig–Sulem formulation. Based on thorough analyses of the Dirichlet–Neumann operators in the long-wave approximation, classic weakly nonlinear models – including the Boussinesq-type system, the Korteweg–de Vries (KdV) equation and its variants, and the Benjamin-type equation – are obtained under different scaling assumptions. In addition, strongly nonlinear models (without the smallness assumption on the wave amplitude) in the Benjamin and Barannyk–Papageorgiou–Petropoulos regimes are derived. In these models, the electric effects are shown to produce dispersive regularisations of long and short waves. A modified boundary integral equation method is developed to compute solitary waves in the original electrified Euler equations. Through comparisons with solitary-wave solutions in the Euler equations, it is found that in various asymptotic regimes, weakly nonlinear models are in overall good agreement when wave amplitudes are small. In contrast, the range of validity of the strongly nonlinear model is much broader. It is shown that the horizontal electric field plays a significant role in the physical system: it expands the range of parameters for the existence of progressive waves, changes the qualitative characteristics of solitary waves and leads to a new type of solitary wave, namely the KdV–wavepacket mixed type.

**Key words:** capillary waves, solitary waves

† Email address for correspondence: [zwang@imech.ac.cn](mailto:zwang@imech.ac.cn)

## 1. Introduction

Electrohydrodynamics, an interdisciplinary subject coupling electrostatic fields into fluid flows through the Maxwell stress tensor, arose in the 1960s when Taylor, Melcher and others began their researches on interfacial hydrodynamic instabilities under electric fields. Motivated by the disintegration of water drops in a strong electric field such as a thunderstorm, Taylor (1964) showed that electrified cones could exist in equilibrium with fixed semi-vertical angle  $49.3^\circ$  (termed the ‘Taylor cone’ in later literature). Subsequently, the destabilising effect of the normal electric field was confirmed by Taylor & McEwan (1965) when they applied it to an extended horizontal surface of a conducting liquid. The normal electric field, which is orthogonal to the undisturbed interface, has a wide range of applications in chemistry and industry, including the cooling system, coating process and microfluidic device, to name a few. Electrospray ionisation resulting from the Taylor cone is an essentially useful technique in converting solution ions into highly charged gas-phase ions of macromolecules (Fernandez de La Mora & Loscertales 1994). It plays a vital role in advanced propulsion and power technologies in space science, such as the field-emission electric propulsion and colloid thrusters used in fine control of spacecraft (see Gamero-Castaño & Hruby (2001) and references therein).

As opposed to the normal electric field causing instability to the fluid layer, the tangential electric field, parallel to the undisturbed interface, has a stabilising effect since it provides a dispersive/dissipative contribution to the linear system (Melcher 1963; Melcher & Schwarz 1968; Kochurin & Zubarev 2018). It can delay the formation of the film rupture (Tilley, Petropoulos & Papageorgiou 2001) and even suppress the Rayleigh–Taylor instability (see Eldabe (1989) for the linear stability analysis). Even in the non-dispersive situation, Zubarev (2004) showed that under a strong tangential electric field, nonlinear wave–wave interactions on a dielectric fluid of infinite depth do not lead to the formation of singularities (say, wave breaking). The control of the Rayleigh–Taylor instability using tangential electric fields has received increasing attention in the past decade due to its potential application in many situations of practical relevance. Joshi, Radhakrishna & Rudraiah (2010) performed the linear stability analysis by involving the polarisation effects and showed how the electrostriction term obliterated the density difference between fluids to remove or delay the instability. For inviscid dielectric fluids, Barannyk, Papageorgiou & Petropoulos (2012) and Barannyk *et al.* (2015) derived reduced nonlinear models based on a multi-scale analysis and showed numerically that instability can be arrested entirely if the tangential electric field is sufficiently strong. Conversely, the touching singularity (i.e. the interface touches the rigid wall) occurs in a finite time when the electric strength is in the subcritical regime. Direct numerical simulations of the full Navier–Stokes equations were carried out by Cimpeanu, Papageorgiou & Petropoulos (2014), Yang *et al.* (2016) and Anderson *et al.* (2017) when gravity, surface tension and tangential electric field were considered. All the groups found complete suppression of the Rayleigh–Taylor instability subject to finite wavelength perturbations.

In this study, two immiscible inviscid fluids with one on top of the other are bounded vertically by two horizontal rigid walls, which are assumed to be electrically insulating (Barannyk *et al.* 2012, 2015). The fluids and electric fields are strongly coupled through the Maxwell stress at the interface (Melcher & Taylor 1969). A horizontally applied electric field, tangent to the undisturbed interface, can exert significant forces competing with gravity and surface tension at the electrified interface when the system is perturbed. Asymptotic modelling and direct numerical simulations of the primitive equations are combined to capture the nonlinear features of electrohydrodynamic waves. Particular attention is paid to new interfacial solitary waves that emerge owing to the

external field. We should emphasise that due to the stabilising effect of horizontal electric fields, the upper fluid layer is allowed to be heavier than the lower layer in modelling and computations.

There have been many studies on asymptotic theories of nonlinear electrohydrodynamic waves propagating at the liquid–gas or liquid–liquid interface in different electrode–fluid configurations for incompressible, inviscid and irrotational flows. Among these works, the long-wave approximation is most commonly examined in the literature. Electrocapillary-gravity waves propagating on the surface of a thin conducting liquid under a normal electric field were studied thoroughly by different groups. When the thickness of the gas layer is of the same order as that of the conducting layer, the celebrated Korteweg–de Vries (KdV) equation with coefficients depending on the electric parameter was obtained by Easwaran (1988). As the top electrode is placed far from the free surface, the Benjamin equation with the electric effect reflected in the term of the Hilbert transform was derived by Gleeson *et al.* (2007) and later on extended to the three-dimensional problem by Hunt *et al.* (2017), which results in the two-dimensional Benjamin equation. Further generalisation was achieved by Wang (2017), who derived bidirectional isotropic models (namely the Benney–Luke-type and Boussinesq-type equations) based on asymptotic expansions of the Dirichlet–Neumann operators in the Hamiltonian framework. When a perfect dielectric liquid replaces the conducting film, the electric field within the fluid domain becomes active and needs to be solved together with other fields. Using matched asymptotic expansions, Papageorgiou, Petropoulos & Vanden-Broeck (2005) and Papageorgiou & Vanden-Broeck (2007) derived reduced integrodifferential systems involving the Hilbert transform while sending the upper electrode to infinity, and computed periodic travelling waves and touch-down dynamics. In the presence of tangential electric fields, coupled evolution equations in the long-wave limit were also obtained and investigated by Tilley *et al.* (2001) and Papageorgiou & Vanden-Broeck (2004a) for the dynamics of electrocapillary waves and by Barannyk *et al.* (2012, 2015) for control of the Rayleigh–Taylor instability. Interested readers are referred to the recent comprehensive review by Papageorgiou (2019) and the references therein for more details about weakly nonlinear models in electrohydrodynamics.

There has been considerable research devoted to fully nonlinear interfacial electrohydrodynamic travelling waves without any assumptions on the size of wave amplitude and wavelength. The conventional tool is solving the electrified Euler equations based on various boundary integral equation methods. When one layer is assumed to be hydrodynamically passive (the gas–liquid interface, for instance), computations of strongly nonlinear travelling waves were carried out by Papageorgiou *et al.* (2005), Papageorgiou & Vanden-Broeck (2007) and Gao *et al.* (2017) for normal electric fields, and by Papageorgiou & Vanden-Broeck (2004a, ) for tangential electric fields. Solutions influenced by surface tension and electrical stress were extended to the axisymmetric configuration by Grandison *et al.* (2007), who showed the existence of travelling toroidal bubbles. When both fluid layers are hydrodynamically active and have the same density, Grandison, Papageorgiou & Vanden-Broeck (2007) computed symmetric and anti-symmetric periodic waves in the presence of a velocity jump across the interface. To the best of our knowledge, no fully nonlinear computations have been performed for the system of two hydrodynamically active dielectrics when the competing forces resulting from gravity, surface tension and electric field are all considered.

In the absence of electric fields, theoretical and numerical aspects of interfacial gravity-capillary waves were investigated by different authors. Benjamin (1992) proposed a weakly nonlinear model, now bearing his name, for long interfacial waves propagating

on an infinitely deep fluid layer assuming small density difference and large interfacial tension between two fluids. He found a new type of solitary wave in the Benjamin equation, bifurcating from infinitesimal periodic waves and featuring oscillatory decaying tails, termed wavepacket solitary waves. Akylas (1993) showed that the existence of wavepacket solitary waves demands a phase speed extremum at a non-zero wavenumber, where the group velocity is equal to the phase velocity. Furthermore, the associated cubic nonlinear Schrödinger (NLS) equation at this particular point is of the focusing type so that soliton solutions of the NLS equation can approximate envelopes of wavepacket solitary waves in the primitive equations. On the other hand, for interfacial gravity-capillary waves between two semi-infinite fluid layers, Laget & Dias (1997) performed the normal-form analysis and found a critical density ratio above which the NLS equation is of defocusing type at the minimum of the phase speed. Unexpectedly, in such a scenario, wavepacket solitary waves were still shown to exist in the full Euler equations but only at finite amplitude. It indicates that the focusing NLS equation is unnecessary for wavepacket solitary waves in the primitive equations. In the present paper, introducing an electric field adds complexity, thereby increasing the difficulty of asymptotic analysis and numerical computations. However, from a linear theory perspective, the horizontal electric field leads to a more complicated dispersion relation. And its stabilising nature expands the range of parameters that can be explored; hence new wave phenomena, particularly new solitary waves, arising from the electric field may be expected.

The main focus of this paper is to quantify nonlinear interfacial electrocapillary-gravity waves between two perfect dielectric liquids, with specific emphasis on solitary waves. The goal is twofold: to propose a systematic way to derive strongly/weakly nonlinear models in different scaling limits, and to provide numerical results for various types of solitary waves in the electrified Euler equations. The rest of the paper is organised as follows. The mathematical formulation of the problem, together with the linear dispersion relation, is described in § 2. Since it is convenient to deal with the problem using interface variables, we reformulate the problem based on the Dirichlet–Neumann operators in the same section. Strongly and weakly nonlinear models are derived in § 3 for different wavelength and amplitude scalings via expanding and truncating the pseudo-differential operators in the kinematic and dynamic boundary conditions. In § 4, solitary waves are solved numerically for the primitive equations based on a boundary integral equation method. Theoretical and numerical solutions of the reduced models are compared with those of the Euler equations, and good agreement is found for small- and moderate-amplitude solitary waves. It is also shown that the electric field has a great impact on the physical system and can change the qualitative nature of the interface. Finally, conclusions and further remarks are given in § 5.

## 2. Mathematical formulation

### 2.1. Governing equations

Two immiscible inviscid incompressible fluids are bound together in an infinite horizontal channel and separated by a sharp interface  $y = \eta(x, t)$ , where  $x$  is the direction of wave propagation, and the  $y$ -axis points upwards, with  $y = 0$  at the undisturbed interface (see the sketch of the system in figure 1). We denote by  $h^\pm$  and  $\rho^\pm$  the depth and density in each layer, where the superscripts ‘+’ and ‘−’ refer to fluid properties associated with the upper and lower fluid layers, respectively. The fluids, which are assumed to be perfect dielectrics with electrical permittivities  $\varepsilon^\pm$ , are under the action of a uniform horizontal electric field of strength  $E_0$  in the absence of perturbations. The flows are supposed to

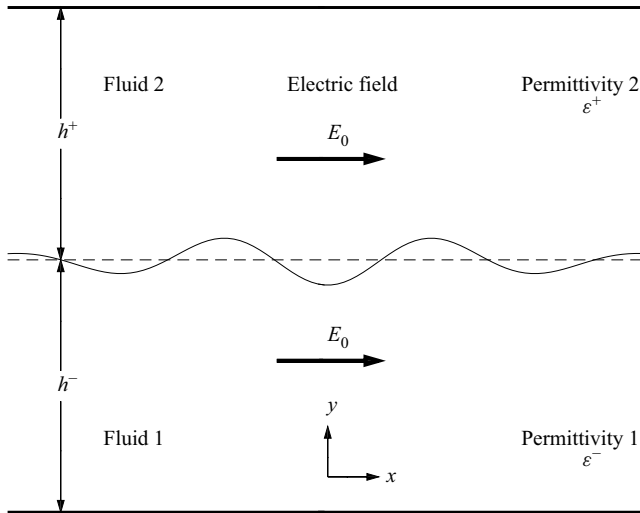


Figure 1. The schematic of the problem. The dashed line represents the undisturbed interface.

be irrotational, hence there exist potential functions  $\phi^\pm$  such that the velocity fields  $\mathbf{u}^\pm$  satisfy  $\mathbf{u}^\pm = \nabla\phi^\pm$ , where  $\nabla = (\partial_x, \partial_y)$  is the gradient operator. If we denote the electric fields by  $E^+$  and  $E^-$  in the corresponding layers, then the electrostatic limit of Maxwell’s equations yields  $\nabla \times E^\pm = 0$ ; therefore voltage potentials  $V^\pm$  can be introduced, such that  $E^\pm = -\nabla V^\pm$ . In this scenario, both velocity potentials and voltage potentials satisfy the Laplace equation:

$$\Delta\phi^+ = 0, \quad \Delta V^+ = 0, \quad \eta < y < h^+, \tag{2.1a,b}$$

$$\Delta\phi^- = 0, \quad \Delta V^- = 0, \quad -h^- < y < \eta, \tag{2.2a,b}$$

where  $\Delta = \partial_{xx} + \partial_{yy}$  is the two-dimensional Laplace operator. The electric fields have to satisfy two boundary conditions at the interface  $y = \eta(x, t)$ , namely the continuity of electric potential and continuity of the electric displacement field given by

$$V^+ = V^-, \quad \epsilon^+ \frac{\partial V^+}{\partial \mathbf{n}} = \epsilon^- \frac{\partial V^-}{\partial \mathbf{n}}, \tag{2.3a,b}$$

where  $\mathbf{n} = (-\eta_x, 1)/\sqrt{1 + \eta_x^2}$  is the unit normal vector pointing outwards from the lower layer. Far away from interfacial disturbances, we should impose the condition

$$V^\pm \rightarrow E_0 x, \quad \text{as } x \rightarrow \pm\infty. \tag{2.4}$$

Following Barannyk *et al.* (2012, 2015), the impermeability conditions should be satisfied for both fluids and electric fields on the channel walls, namely

$$\left. \begin{aligned} \frac{\partial\phi^+}{\partial y} = \frac{\partial V^+}{\partial y} = 0, \quad \text{at } y = h^+, \\ \frac{\partial\phi^-}{\partial y} = \frac{\partial V^-}{\partial y} = 0, \quad \text{at } y = h^-. \end{aligned} \right\} \tag{2.5}$$

On physical grounds, the no-current boundary condition for electric fields is used to model electrically insulating walls. The hydrodynamic boundary conditions at the interface are a

kinematic condition

$$\eta_t = \phi_y^+ - \eta_x \phi_x^+ = \phi_y^- - \eta_x \phi_x^-, \tag{2.6}$$

which indicates continuity of normal velocity, and a modified dynamic boundary condition resulting from pressure continuity across the interface:

$$\begin{aligned} &\rho^- \left( \phi_t^- + \frac{1}{2} |\nabla \phi^-|^2 + g\eta \right) - \rho^+ \left( \phi_t^+ + \frac{1}{2} |\nabla \phi^+|^2 + g\eta \right) \\ &+ [\mathbf{n} \cdot \Sigma \cdot \mathbf{n}]_+^- - \frac{\sigma \eta_{xx}}{(1 + \eta_x^2)^{3/2}} = 0, \end{aligned} \tag{2.7}$$

where  $g$  is the acceleration due to gravity,  $\sigma$  is the coefficient of surface tension,  $\mathbf{n} \cdot \Sigma \cdot \mathbf{n}$  arises from the Maxwell stress tensor  $(\Sigma_{ij})_{i,j=1,2}$  given by

$$\Sigma_{11} = \frac{\varepsilon}{2}(V_x^2 - V_y^2), \quad \Sigma_{12} = \Sigma_{21} = \varepsilon V_x V_y, \quad \Sigma_{22} = \frac{\varepsilon}{2}(V_y^2 - V_x^2), \tag{2.8a-c}$$

and  $[\cdot]_+^-$  represents the jump in this quantity across the interface. A straightforward calculation yields

$$[\mathbf{n} \cdot \Sigma \cdot \mathbf{n}]_+^- = \varepsilon^- \left[ \left( \frac{\partial V^-}{\partial \mathbf{n}} \right)^2 - \frac{1}{2} |\nabla V^-|^2 \right] - \varepsilon^+ \left[ \left( \frac{\partial V^+}{\partial \mathbf{n}} \right)^2 - \frac{1}{2} |\nabla V^+|^2 \right]. \tag{2.9}$$

For convenience, we introduce new functions  $W^\pm = V^\pm/E_0 - x$ , hence  $W^\pm \rightarrow 0$  as  $x \rightarrow \pm\infty$ , and  $W^\pm$  still satisfy Laplace’s equation. Therefore, (2.3a,b) and (2.9) can be rewritten as

$$(\varepsilon^+ - \varepsilon^-)\eta_x = \varepsilon^+(W_y^+ - \eta_x W_x^+) - \varepsilon^-(W_y^- - \eta_x W_x^-), \tag{2.10}$$

$$\begin{aligned} [\mathbf{n} \cdot \Sigma \cdot \mathbf{n}]_+^- &= E_0^2 \varepsilon^- \left[ \left( \frac{\partial W^-}{\partial \mathbf{n}} \right)^2 - \frac{1}{2} |\nabla W^-|^2 \right] - E_0^2 (\varepsilon^- W_x^- - \varepsilon^+ W_x^+) \\ &\quad - E_0^2 \varepsilon^+ \left[ \left( \frac{\partial W^+}{\partial \mathbf{n}} \right)^2 - \frac{1}{2} |\nabla W^+|^2 \right] + \frac{E_0^2 (\varepsilon^+ - \varepsilon^-) \eta_x^2}{1 + \eta_x^2}, \end{aligned} \tag{2.11}$$

respectively, where the constant  $E_0^2(\varepsilon^+ - \varepsilon^-)$  in (2.11) has been neglected since it can always be absorbed by redefining  $\phi^\pm$  in the dynamic boundary condition. Finally, (2.1a,b), (2.2a,b), (2.5), (2.6), (2.7), (2.10) and the continuity condition  $W^+ = W^-$  at the interface complete the whole problem.

### 2.2. Zakharov–Craig–Sulem formulation

The Dirichlet–Neumann operator (DNO), which sends boundary value data to normal derivative data via solving the Laplace equation, is essential for investigating free boundary problems in potential theory. We define the velocity potentials and voltage

potential at the interface as

$$\left. \begin{aligned} \xi^+(x, t) &= \phi^+(x, \eta(x, t), t), & \xi^-(x, t) &= \phi^-(x, \eta(x, t), t), \\ W(x, t) &= W^+(x, \eta(x, t), t) = W^-(x, \eta(x, t), t). \end{aligned} \right\} \quad (2.12)$$

First, it follows from the kinematic boundary condition and the definitions of  $\xi^\pm$  that at the interface,

$$\phi_x^\pm = \frac{\xi_x^\pm - \eta_x \eta_t}{1 + \eta_x^2} \quad \text{and} \quad \phi_y^\pm = \frac{\eta_t + \eta_x \xi_x^\pm}{1 + \eta_x^2}. \quad (2.13a,b)$$

Following Craig & Sulem (1993), we introduce the DNOs

$$\left. \begin{aligned} G^+(\eta, h^+) \xi^+ &= [\eta_x \phi_x^+ - \phi_y^+]_{y=\eta} = [\nabla \phi^+ \cdot (-\mathbf{n}) \sqrt{1 + \eta_x^2}]_{y=\eta}, \\ G^-(\eta, h^-) \xi^- &= [\phi_y^- - \eta_x \phi_x^-]_{y=\eta} = [\nabla \phi^- \cdot \mathbf{n} \sqrt{1 + \eta_x^2}]_{y=\eta}, \\ G^+(\eta, h^+) W &= [\eta_x W_x^+ - W_y^+]_{y=\eta} = [\nabla W^+ \cdot (-\mathbf{n}) \sqrt{1 + \eta_x^2}]_{y=\eta}, \\ G^-(\eta, h^-) W &= [W_y^- - \eta_x W_x^-]_{y=\eta} = [\nabla W^- \cdot \mathbf{n} \sqrt{1 + \eta_x^2}]_{y=\eta}. \end{aligned} \right\} \quad (2.14)$$

We suppress the dependency of DNOs on  $h^\pm$  and  $\eta$  in subsequent analyses for simplicity of notation. Then the derivatives of  $W^\pm$  can be expressed as

$$W_x^\pm = \frac{W_x \pm \eta_x G^\pm W}{1 + \eta_x^2} \quad \text{and} \quad W_y^\pm = \frac{\mp G^\pm W + \eta_x W_x}{1 + \eta_x^2}, \quad (2.15a,b)$$

the kinematic boundary condition can be rewritten as a compact form

$$\eta_t = G^- \xi^- = -G^+ \xi^+, \quad (2.16)$$

and the continuity equation for the electric displacement field at the interface now reads

$$\varepsilon^- G^- W + \varepsilon^+ G^+ W = (\varepsilon^- - \varepsilon^+) \eta_x. \quad (2.17)$$

Following Zakharov (1968), who formulated the free-surface water wave problem in terms of surface quantities, we can rewrite the pressure equation as

$$\begin{aligned} &\rho^- \left[ \xi_t^- + \frac{1}{2} (\xi_x^-)^2 - \frac{(\eta_t + \eta_x \xi_x^-)^2}{2(1 + \eta_x^2)} \right] - \rho^+ \left[ \xi_t^+ + \frac{1}{2} (\xi_x^+)^2 - \frac{(\eta_t + \eta_x \xi_x^+)^2}{2(1 + \eta_x^2)} \right] \\ &+ \frac{E_0^2}{2(1 + \eta_x^2)} [\varepsilon^- (G^- W)^2 - \varepsilon^+ (G^+ W)^2 - (\varepsilon^- - \varepsilon^+) (W_x^2 + 2W_x \eta_x)] \\ &+ (\rho^- - \rho^+) g \eta - \frac{\sigma \eta_{xx}}{(1 + \eta_x^2)^{3/2}} = 0, \end{aligned} \quad (2.18)$$

upon substituting (2.11), (2.13a,b), and (2.15a,b) into (2.7), and noticing that  $\xi_t^\pm = \phi_t^\pm + \eta_t \phi_y^\pm$ . We denote by  $\xi = \rho^- \xi^- - \rho^+ \xi^+$  the potential difference at the interface, and it is easy to see that (2.18) is the evolution equation for  $\xi$ . Recalling the kinematic boundary

condition (2.16), one obtains the relations between  $\xi$  and  $\xi^\pm$  as

$$G^+ \xi = (\rho^- G^+ + \rho^+ G^-) \xi^- \implies \xi^- = (\rho^- G^+ + \rho^+ G^-)^{-1} G^+ \xi, \tag{2.19}$$

$$G^- \xi = -(\rho^- G^+ + \rho^+ G^-) \xi^+ \implies \xi^+ = -(\rho^- G^+ + \rho^+ G^-)^{-1} G^- \xi. \tag{2.20}$$

On the other hand, due to (2.17), the voltage potential  $W$  and the interface displacement are related through

$$W = (\varepsilon^- - \varepsilon^+) (\varepsilon^- G^- + \varepsilon^+ G^+)^{-1} \eta_x. \tag{2.21}$$

Finally, by replacing  $\xi^\pm$  and  $W$  with (2.19)–(2.21), equations (2.16) and (2.18) form a closed system with two unknowns:  $\eta$  and  $\xi$ .

### 2.3. Linear theory

Coifman & Meyer (1985) proved that if the  $L^1$ -norm and Lipschitz-norm of  $\eta$  are smaller than a certain constant, then  $G^-$  is an analytic function of  $\eta$ . It then follows that  $G^-(\eta, h^-)$  can be written naturally in the form of a Taylor expansion in  $\eta$ , namely  $G^-(\eta, h^-) = \sum_{j=0}^\infty G_j^-(\eta, h^-)$ , and Craig & Sulem (1993) initially obtained a recursive formula for the expansion. The first three terms of the Taylor series are given by

$$\left. \begin{aligned} G_0^- &= (-\partial_{xx})^{1/2} \tanh((-\partial_{xx})^{1/2} h^-), \\ G_1^- &= -\partial_x \eta \partial_x - G_0^- \eta G_0^-, \\ G_2^- &= \frac{1}{2} G_0^- \eta^2 \partial_{xx} + \frac{1}{2} \partial_{xx} \eta^2 G_0^- + G_0^- \eta G_0^- \eta G_0^-, \end{aligned} \right\} \tag{2.22}$$

where the dependency of  $G_j^-$  on  $\eta$  and  $h^-$  has been suppressed for simplicity as usual. In the same vein, the DNO for the upper-layer fluid,  $G^+(\eta, h^+)$ , can be expanded as

$$G^+(\eta, h^+) = \sum_{j=0}^\infty G_j^+(\eta, h^+) = \sum_{j=0}^\infty (-1)^j G_j^-(\eta, h^+), \tag{2.23}$$

which is obtained by replacing  $\eta$  and  $h^-$  with  $-\eta$  and  $h^+$ , respectively, in  $G_j^-(\eta, h^-)$ .

In the subsequent analyses, we derive the linear dispersion relation of the problem. We first linearise the whole system around the trivial uniform stream solution  $\eta = \phi = W = 0$ . Dropping nonlinear terms in (2.16), (2.18) and (2.21) gives

$$\left. \begin{aligned} \eta_t &= G_0^- (\rho^- G_0^+ + \rho^+ G_0^-)^{-1} G_0^+ \xi, \\ \xi_t - E_0^2 (\varepsilon^- - \varepsilon^+) W_x + (\rho^- - \rho^+) g \eta - \sigma \eta_{xx} &= 0, \\ W &= (\varepsilon^- - \varepsilon^+) (\varepsilon^- G_0^- + \varepsilon^+ G_0^+)^{-1} \eta_x. \end{aligned} \right\} \tag{2.24}$$

For wavenumber  $k$  and frequency  $\omega$ , substituting the ansatz

$$(\eta, \xi, W) = (\hat{\eta}, \hat{\xi}, \hat{W}) e^{i(kx - \omega t)}, \tag{2.25}$$

into the system (2.24) yields

$$\left. \begin{aligned} -i\omega \hat{\eta} &= \frac{|k| \tanh(|k|h^-) \tanh(|k|h^+)}{\rho^- \tanh(|k|h^+) + \rho^+ \tanh(|k|h^-)} \hat{\xi}, \\ [\varepsilon^+ |k| \tanh(|k|h^+) + \varepsilon^- |k| \tanh(|k|h^-)] \hat{W} &= (\varepsilon^- - \varepsilon^+) ik \hat{\eta}, \\ -i\omega \hat{\xi} + (\rho^- - \rho^+) g \hat{\eta} - E_0^2 (\varepsilon^- - \varepsilon^+) ik \hat{W} + \sigma k^2 \hat{\eta} &= 0. \end{aligned} \right\} \tag{2.26}$$



This is a homogeneous linear algebraic system for  $\hat{\eta}$ ,  $\hat{\xi}$  and  $\hat{W}$ . By requiring the solution for this system to be non-trivial, we obtain, after some algebra, the linear dispersion relation in the form

$$\omega^2 = \frac{|k| \tanh(|k|h^-) \tanh(|k|h^+)}{\mathcal{A}(|k|)} \left[ (\rho^- - \rho^+)g + \frac{E_0^2(\varepsilon^- - \varepsilon^+)^2|k|}{\mathcal{B}(|k|)} + \sigma|k|^2 \right], \quad (2.27)$$

with

$$\mathcal{A}(|k|) = \rho^- \tanh(|k|h^+) + \rho^+ \tanh(|k|h^-), \quad (2.28)$$

$$\mathcal{B}(|k|) = \varepsilon^+ \tanh(|k|h^+) + \varepsilon^- \tanh(|k|h^-). \quad (2.29)$$

In the long-wave regime, i.e. the wavenumber  $k$  is close to zero, the dispersion relation (2.27) can be approximated by

$$\omega^2 \approx \frac{h^- h^+}{\rho^- h^+ + \rho^+ h^-} \left[ \rho^- - \rho^+ + \frac{E_0^2(\varepsilon^- - \varepsilon^+)^2}{\varepsilon^+ h^+ + \varepsilon^- h^-} \right] |k|^2, \quad (2.30)$$

which shows clearly the stabilising effect of the electric field. However, if one of the fluid layers is of infinite depth, then the electric field can provide dispersive regularisation only to short waves. For example, we let  $h^- \rightarrow \infty$ , and then the leading-order dispersion relation near  $k = 0$  reads  $\omega^2 \approx |k|^2(\rho^- - \rho^+)h^+/\rho^+$ , indicating that the system is linearly ill-posed when  $\rho^+ > \rho^-$  (namely the Rayleigh–Taylor unstable regime).

### 3. Long-wave modelling

In this section, various nonlinear long-wave models are derived via systematic asymptotic analyses of the DNOs in the Zakharov–Craig–Sulem formulation of the problem. Our analyses will be based on a fundamental assumption that the lower layer is thin compared with a characteristic wavelength. Due to the long-wave assumption, a small parameter measuring the aspect ratio of vertical to horizontal scales,  $\mu = h^-/\lambda \ll 1$ , can be introduced, where  $\lambda$  is a characteristic wavelength. Further asymptotic limits imposed on the thickness of the upper layer (shallow/deep in comparison with the typical wavelength) can lead to different reduced models. These models will be used in the next section to validate the numerical algorithm for the full Euler equations and provide quantitative/qualitative understandings of solitary-wave solutions under the horizontal electric field.

It is convenient to choose  $h^-$ ,  $\sqrt{gh^-}$  and  $\sqrt{g(h^-)^3}$  as reference scales of length, velocity and potential, and denote by

$$h = h^+ / h^-, \quad R = \rho^+ / \rho^-, \quad \varepsilon = \varepsilon^+ / \varepsilon^-, \quad (3.1a-c)$$

the ratios of depth, density and permittivity. The dimensionless dynamic boundary condition now reads

$$\begin{aligned} \xi_t + \frac{1}{2} \left[ (\xi_x^-)^2 - \frac{(\eta_t + \eta_x \xi_x^-)^2}{1 + \eta_x^2} \right] - \frac{R}{2} \left[ (\xi_x^+)^2 - \frac{(\eta_t + \eta_x \xi_x^+)^2}{1 + \eta_x^2} \right] \\ + \frac{E_b}{2(1 + \eta_x^2)} [(G^- W)^2 - \varepsilon(G^+ W)^2 - (1 - \varepsilon)(W_x^2 + 2W_x)] \\ + (1 - R)\eta - \frac{\tau \eta_{xx}}{(1 + \eta_x^2)^{3/2}} = 0, \end{aligned} \quad (3.2)$$

where  $\xi$  has been redefined as  $\xi = \xi^- - R\xi^+$ ,  $E_b = E_0^2 \varepsilon^- / \rho^- g h^-$  is an electric Bond number (the ratio of the electric to gravitational forces), and  $\tau = \sigma / \rho^- g (h^-)^2$  is the traditional Bond number (the ratio of the capillary to gravitational forces). It is noted that the thickness of the lower layer has been normalised to unity, while the kinematic boundary condition (2.16) is unchanged after the non-dimensionalisation.

### 3.1. Equations for the shallow–shallow configuration

In what follows, we analyse the problem when the thickness of the upper fluid layer is comparable to that of the lower layer, namely  $h = h^+ / h^- = O(1)$ . This means that both layers are shallow in comparison with the typical length of the interfacial wave. We derive weakly nonlinear models in various asymptotic regimes, each of which features a nonlinearity–dispersion balance.

We first consider the classic Boussinesq scaling: the interfacial wave varies on temporal and horizontal spatial scales of  $1/\mu$ , and the amplitude of the interface displacement scales by  $\mu^2$ . All the parameters, including the Bond number, electric Bond number, depth ratio and permittivity ratio, are assumed to be of order  $\mu^0$  to enable the forces exerted by the electric field, surface tension and gravity to compete with each other. In summary, the following scales are chosen:

$$\left. \begin{aligned} \partial_x = O(\mu), \quad \partial_t = O(\mu), \quad \eta = O(\mu^2), \quad \xi = O(\mu), \\ R = O(1), \quad E_b = O(1), \quad \tau = O(1), \quad \varepsilon = O(1). \end{aligned} \right\} \quad (3.3)$$

We use order-of-magnitude arguments to derive reduced nonlinear models. First, due to the smallness of the spatial derivative, the DNOs can be expanded as

$$\left. \begin{aligned} G^- &= -\partial_{xx} - \frac{1}{3} \partial_{xxxx} - \partial_x \eta \partial_x + O(\mu^6), \\ G^+ &= -h \partial_{xx} - \frac{h^3}{3} \partial_{xxxx} + \partial_x \eta \partial_x + O(\mu^6), \end{aligned} \right\} \quad (3.4)$$

and then a direct symbolic calculation yields

$$\begin{aligned} (G^+ + R G^-)^{-1} &= \left\{ -(h + R) \partial_{xx} \left[ 1 + \frac{h^3 + R}{3(h + R)} \partial_{xx} - \frac{1 - R}{h + R} \partial_x^{-1} \eta \partial_x + O(\mu^4) \right] \right\}^{-1} \\ &= -\frac{1}{h + R} \left[ 1 + \frac{h^3 + R}{3(h + R)} \partial_{xx} - \frac{1 - R}{h + R} \partial_x^{-1} \eta \partial_x + O(\mu^4) \right]^{-1} \partial_{xx}^{-1} \\ &= -\frac{\partial_{xx}^{-1}}{h + R} + \frac{h^3 + R}{3(h + R)^2} - \frac{1 - R}{(h + R)^2} \partial_x^{-1} \eta \partial_x^{-1} + O(\mu^2). \end{aligned} \quad (3.5)$$

In the same vein, one can obtain

$$(\varepsilon G^+ + G^-)^{-1} = -\frac{\partial_{xx}^{-1}}{\varepsilon h + 1} + \frac{\varepsilon h^3 + 1}{3(\varepsilon h + 1)^2} + \frac{1 - \varepsilon}{(\varepsilon h + 1)^2} \partial_x^{-1} \eta \partial_x^{-1} + O(\mu^2). \quad (3.6)$$

With the aid of these formulae, we have the following expansions, after some calculations of (2.19)–(2.21):

$$\xi^- = \frac{h \xi}{h + R} + O(\mu^2), \quad \xi^+ = \frac{\xi}{h + R} + O(\mu^2), \quad (3.7a,b)$$

and

$$W_x = -\frac{1 - \varepsilon}{\varepsilon h + 1} \eta + \frac{(1 - \varepsilon)(\varepsilon h^3 + 1)}{3(\varepsilon + 1)^2} \eta_{xx} + \frac{(1 - \varepsilon)^2}{(\varepsilon h + 1)^2} \eta^2 + O(\mu^4). \quad (3.8)$$

Substituting the above formulae into boundary conditions at the interface, and retaining terms valid up to  $O(\mu^5)$  in (2.16) and  $O(\mu^4)$  in (3.2), one then obtains

$$\eta_t = -\frac{h}{h + R} \xi_{xx} - \frac{h^2(1 + hR)}{3(h + R)^2} \xi_{xxx} - \frac{h^2 - R}{(h + R)^2} (\eta \xi_x)_x, \quad (3.9)$$

$$\begin{aligned} \xi_t = & -\left[1 - R + \frac{E_b(1 - \varepsilon)^2}{\varepsilon h + 1}\right] \eta - \frac{h^2 - R}{2(h + R)^2} \xi_x^2 + \frac{3E_b(1 - \varepsilon)^3}{2(\varepsilon h + 1)^2} \eta^2 \\ & + \left[\frac{E_b(1 - \varepsilon)^2(\varepsilon h^3 + 1)}{3(\varepsilon h + 1)^2} + \tau\right] \eta_{xx}, \end{aligned} \quad (3.10)$$

a Boussinesq-type system in the presence of a horizontal electric field. From the system (3.9) and (3.10), we can infer that the electric field can provide dispersive regularisation to both gravity and surface tension, and introduce new nonlinearity.

The KdV equation can be derived from (3.9) and (3.10) upon further simplifications. Taking the derivative of (3.10) with respect to  $x$  yields

$$\eta_t + u_x = -\frac{h(1 + hR)}{3(h + R)} u_{xxx} - \frac{h^2 - R}{h(h + R)} (\eta u)_x, \quad (3.11)$$

$$\begin{aligned} u_t + c^2 \eta_x = & -\frac{h^2 - R}{2h(h + R)} (u^2)_x + \frac{3hE_b(1 - \varepsilon)^3}{2(\varepsilon h + 1)^2(h + R)} (\eta^2)_x \\ & + \frac{h}{h + R} \left[\frac{E_b(1 - \varepsilon)^2(\varepsilon h^3 + 1)}{3(\varepsilon h + 1)^2} + \tau\right] \eta_{xxx}, \end{aligned} \quad (3.12)$$

where

$$u = \frac{h\xi_x}{h + R} \quad \text{and} \quad c^2 = \frac{h}{h + R} \left[1 - R + \frac{E_b(1 - \varepsilon)^2}{\varepsilon h + 1}\right]. \quad (3.13a,b)$$

Note that the leading order of the system is a classic wave equation  $\eta_{tt} - c^2 \eta_{xx} = 0$ . Assuming that the wave travels mainly towards one direction (say, the right direction), the solution must take the form  $\eta(x - ct) + \dots$ , and it then follows that  $u = c\eta + \tilde{u}(x - ct)$ , where  $\tilde{u}$  is of order  $\mu^4$ . Upon substituting  $u$  with  $c\eta + \tilde{u}$  in (3.11) and (3.12), and eliminating the leading-order terms via subtracting one equation from the other, we find

$$\begin{aligned} \tilde{u} = & -\frac{h}{2c(h + R)} \left[\frac{c^2(1 + hR)}{3} + \frac{E_b(1 - \varepsilon)^2(\varepsilon h^3 + 1)}{3(\varepsilon h + 1)^2} + \tau\right] \eta_{xx} \\ & - \frac{1}{2c} \left[\frac{c^2(h^2 - R)}{2h(h + R)} + \frac{3hE_b(1 - \varepsilon)^3}{2(\varepsilon h + 1)^2(h + R)}\right] \eta^2. \end{aligned} \quad (3.14)$$

Finally, substituting (3.14) into (3.11) or (3.12) yields the KdV equation

$$\eta_t + c\eta_x + \alpha \eta_{xxx} + \beta \eta \eta_x = 0, \quad (3.15)$$

where

$$\alpha = -\frac{h}{2c(h+R)} \left[ \frac{E_b(1-\varepsilon)^2(\varepsilon h^3 + 1)}{3(\varepsilon h + 1)^2} + \tau - \frac{c^2(1+hR)}{3} \right], \tag{3.16}$$

$$\beta = \frac{3}{2c} \left[ \frac{c^2(h^2 - R)}{h(h+R)} - \frac{hE_b(1-\varepsilon)^3}{(\varepsilon h + 1)^2(h+R)} \right], \tag{3.17}$$

are the dispersive and nonlinear coefficients, respectively. The famous soliton solution admitted by (3.15) is given by

$$\eta = \frac{12\alpha}{\beta} \delta^2 \operatorname{sech}^2[\delta(x - ct - 4\delta^2\alpha t - x_0)], \tag{3.18}$$

where  $\delta$  and  $x_0$  are arbitrary constants associated with the wave amplitude and initial phase, respectively.

It is well known that the soliton formation arises from a dynamic balance between dispersive and nonlinear effects. However, the dispersive and nonlinear coefficients in (3.15),  $\alpha$  and  $\beta$ , may be close to zero for certain parameter sets, hence rescaling is required in the asymptotic analysis. For the first case,  $\beta \ll 1$ , a higher-order nonlinearity needs to be introduced to balance the dispersion, resulting in the modified KdV equation. For this purpose, we choose the scales

$$\partial_x = O(\mu), \quad \partial_t = O(\mu), \quad \eta = O(\mu), \quad \xi = O(1), \quad \beta = O(\mu), \tag{3.19a-e}$$

and the other parameters ( $h$ ,  $R$ ,  $\varepsilon$  and  $E_b$ ) keep the original order of magnitude. The new scaling indicates that the balance between the two effects can be achieved for larger-amplitude waves, though the temporal and spatial scales for solitons remain the same. Following the same procedure, symbolic calculations yield

$$\left. \begin{aligned} \xi_x^- &= \frac{h}{h+R} \xi_x - \frac{R(1+h)}{(R+h)^2} \eta \xi_x + O(\mu^3), \\ \xi_x^+ &= -\frac{1}{h+R} \xi_x - \frac{1+h}{(R+h)^2} \eta \xi_x + O(\mu^3), \\ W_x &= -\frac{1-\varepsilon}{1+\varepsilon h} \eta + \frac{(1-\varepsilon)^2}{(1+\varepsilon h)^2} \eta^2 + \frac{(1-\varepsilon)(1+\varepsilon h^3)}{3(1+\varepsilon h)^2} \eta_{xx} - \frac{(1-\varepsilon)^3}{(1+\varepsilon h)^3} \eta^3 + O(\mu^4). \end{aligned} \right\} \tag{3.20}$$

Substituting the above formulae into the kinematic and dynamic boundary conditions, namely (2.16) and (3.2), and then truncating the expansions at appropriate orders in  $\mu$ , one obtains

$$\eta_t = -\frac{h}{h+R} \xi_{xx} + \frac{R-h^2}{(h+R)^2} (\eta \xi_x)_x - \frac{h^2(1+hR)}{3(h+R)^2} \xi_{xxx} + \frac{R(1+h)^2}{(h+R)^3} (\eta^2 \xi_x)_x, \tag{3.21}$$

$$\begin{aligned} \xi_t &= -\left[ 1 - R + \frac{E_b(1-\varepsilon)^2}{1+\varepsilon h} \right] \eta + \frac{R-h^2}{2(h+R)^2} \xi_x^2 + \frac{3E_b(1-\varepsilon)^3}{2(1+\varepsilon h)^2} \eta^2 \\ &+ \left[ \frac{E_b(1-\varepsilon)^2(1+\varepsilon h^3)}{3(1+\varepsilon h)^2} + \tau \right] \eta_{xx} + \frac{R(1+h)^2}{(h+R)^3} \eta \xi_x^2 - \frac{2E_b(1-\varepsilon)^4}{(1+\varepsilon h)^3} \eta^3. \end{aligned} \tag{3.22}$$

By assuming one-way wave propagation along a major direction (right-going waves, say) and following a standard argument, one finally, after some tedious calculation, obtains a

modified KdV equation

$$\eta_t + c\eta_x + \alpha\eta_{xxx} + \beta\eta\eta_x + \tilde{\beta}\eta^2\eta_x = 0, \tag{3.23}$$

where  $c$  is the long-wave speed defined in (3.13a,b),  $\alpha$  and  $\beta$  are the same as given in (3.16) and (3.17), and

$$\tilde{\beta} = \frac{3hE_b(1-\varepsilon)^4}{c(1+\varepsilon h)^3(h+R)} + \frac{3E_b(1-\varepsilon)^3(R-h^2)}{c(1+\varepsilon h)^2(h+R)^2} - \frac{3cR(1+h)^2}{h(h+R)^2}. \tag{3.24}$$

For the second case,  $\alpha \ll 1$ , a fifth-order derivative term is commonly introduced to balance the quadratic nonlinearity, implying the scaling

$$\partial_x = O(\mu), \quad \partial_t = O(\mu), \quad \eta = O(\mu^4), \quad \xi = O(\mu^3), \quad \alpha = O(\mu^2). \tag{3.25a-e}$$

Following the same argument, after some algebra, a fifth-order KdV equation can be obtained to govern the interface dynamics:

$$\eta_t + c\eta_x + \alpha\eta_{xxx} + \beta\eta\eta_x + \tilde{\alpha}\eta_{xxxxx} = 0, \tag{3.26}$$

where

$$\begin{aligned} \tilde{\alpha} = & \frac{hc}{h+R} \left[ \frac{1+h^3R}{15} - \frac{R(1-h^2)^2}{18(h+R)} \right] - \frac{h^2(1+hR)\tau}{6c(h+R)^2} \\ & + \frac{hE_b(1-\varepsilon)^2}{2c(h+R)} \left[ \frac{(1+\varepsilon h^3)^2}{9(1+\varepsilon h)^3} - \frac{2(1+\varepsilon h^5)}{15(1+\varepsilon h)^2} - \frac{h(1+hR)(1+\varepsilon h^3)}{9(h+R)(1+\varepsilon h)^2} \right]. \end{aligned} \tag{3.27}$$

There is a third possibility:  $\alpha$  and  $\beta$  are very close to zero for the same set of parameters. This is possible even when the electric field is absent, as long as one chooses  $R \approx h^2$  and  $\tau \approx (1-h)(1+h^3)/3$ . In this situation, one can obtain a higher-order modified KdV equation, including fifth-order dispersion and cubic nonlinearity (see Laget & Dias (1997) for the case when the electric field is absent). We omit the derivation of the model equation since it is tedious but straightforward if one follows the previous procedure.

### 3.2. Equation for the case of great upper-layer depth

In this part, we consider the case that the typical wavelength  $\lambda$  is much larger than the mean depth of the lower layer but comparable to the thickness of the upper layer, which is termed the Benjamin scaling. The non-dimensionalisation is achieved in the same way as in the shallow–shallow case, where  $h^-$  is taken as the length scale. Based on the linear analysis,  $R$  is always set to be less than 1 in the current subsection, such that the problem is linearly well-posed. The Benjamin regime includes the additional expectation of small-amplitude motions and large interfacial tension (Benjamin 1992). One chooses the scaling

$$\left. \begin{aligned} \partial_x = O(\mu), \quad \partial_t = O(\mu), \quad \eta = O(\mu), \quad \xi = O(1), \quad h \geq O(1/\mu), \\ R = O(1), \quad \varepsilon = O(1), \quad E_b = O(1), \quad \tau = O(1/\mu). \end{aligned} \right\} \tag{3.28}$$

In this case, the expansions of the DNOs can be expressed as

$$G^- = -\partial_{xx} - \frac{1}{3}\partial_{xxxx} - \partial_x\eta\partial_x + O(\mu^6), \tag{3.29}$$

$$G^+ = G_0^+ + \partial_x\eta\partial_x + G_0^+\eta G_0^+ + O(\mu^5), \tag{3.30}$$

where

$$G_0^+ = (-\partial_{xx})^{1/2} \tanh(h(-\partial_{xx})^{1/2}) = O(\mu). \tag{3.31}$$

It then follows that

$$(G^+ + RG^-)^{-1} = (G_0^+)^{-1} + R(G_0^+)^{-1} \partial_{xx} (G_0^+)^{-1} + O(\mu), \tag{3.32}$$

$$(\varepsilon G^+ + G^-)^{-1} = \frac{1}{\varepsilon} (G_0^+)^{-1} + O(1). \tag{3.33}$$

Substituting these expansions into boundary conditions at the interface gives

$$\eta_t = -\xi_{xx} - (\eta \xi_x)_x - R \mathcal{P} \xi_{xxx}, \tag{3.34}$$

$$\xi_t = -\frac{1}{2} \xi_x^2 + \frac{E_b(1-\varepsilon)^2}{\varepsilon} \mathcal{P} \eta_x - (1-R)\eta + \tau \eta_{xx}, \tag{3.35}$$

where  $\mathcal{P} = \partial_x (G_0^+)^{-1}$  is a pseudo-differential operator. In the limiting case  $h \rightarrow \infty$ , this operator becomes the Hilbert transform  $\mathcal{H}$  defined by

$$\mathcal{H}[f](x) = \frac{1}{\pi} \text{P.V.} \int \frac{f(x')}{x' - x} dx', \tag{3.36}$$

where ‘P.V.’ means that the integral is in the Cauchy principal value sense. Finally, by assuming one-way wave propagation and following the same procedure as the previous subsection, one can reduce the system to a single evolution equation for  $\eta$ :

$$\eta_t + c \eta_x + \frac{3c}{2} \eta \eta_x + \left[ \frac{cR}{2} - \frac{E_b(1-\varepsilon)^2}{2\varepsilon c} \right] \mathcal{P} \eta_{xx} - \frac{\tau}{2c} \eta_{xxx} = 0, \tag{3.37}$$

where  $c = \sqrt{1-R}$  is the long-wave speed. For the limiting case  $h \rightarrow \infty$ , (3.37) reduces to the famous Benjamin equation for long interfacial waves with strong surface tension (Benjamin 1992). In the context of electrohydrodynamic waves, the Benjamin equation was first derived by Gleeson *et al.* (2007), who investigated the free-surface evolution of a conducting fluid under a normal electric field.

While weakly nonlinear dispersive models, such as (3.37), have been successful in many aspects of the free-surface/interfacial wave problems, strongly nonlinear models still need to be developed to describe moderate-amplitude wave phenomena as well as to afford a significant simplification over the primitive equations. Next, we derive strongly nonlinear models without the smallness assumption on the wave amplitude. The following scaling is made:

$$\left. \begin{aligned} \partial_x &= O(\mu), & \partial_t &= O(\mu), & \eta &= O(1), & \xi &= O(1/\mu), \\ R &= O(1), & \varepsilon &= O(1), & E_b &= O(1), & \tau &= O(1/\mu). \end{aligned} \right\} \tag{3.38}$$

Under this scaling assumption, one proceeds by expanding the DNOs in powers of  $\mu$ :

$$G^- = -\partial_{xx} - \partial_x \eta \partial_x + O(\mu^4), \tag{3.39}$$

$$G^+ = G_0^+ + \partial_x \eta \partial_x + G_0^+ \eta G_0^+ + O(\mu^3). \tag{3.40}$$

We can then expand the crucial pseudo-differential operator  $(G^+ + RG^-)^{-1}$  symbolically as

$$\begin{aligned} (G^+ + RG^-)^{-1} &= [G_0^+ + \partial_x \eta \partial_x + G_0^+ \eta G_0^+ - R \partial_{xx} - R \partial_x \eta \partial_x + O(\mu^3)]^{-1} \\ &= (G_0^+)^{-1} - \eta - (1-R)(G_0^+)^{-1} \partial_x \eta \partial_x (G_0^+)^{-1} + R(G_0^+)^{-2} \partial_{xx} + O(\mu). \end{aligned} \tag{3.41}$$

Similarly, we have

$$(\varepsilon G^+ + G^-)^{-1} = \frac{1}{\varepsilon} (G_0^+)^{-1} + O(1) \implies W_x = \frac{1 - \varepsilon}{\varepsilon} (G_0^+)^{-1} \partial_{xx} \eta + O(\mu^2), \quad (3.42)$$

and

$$\xi^- = \xi + R(G_0^+)^{-1} \partial_{xx} \xi + R(G_0^+)^{-1} \partial_x \eta \partial_x \xi + O(\mu), \quad (3.43)$$

$$\xi^+ = (G_0^+)^{-1} \partial_{xx} \xi + (G_0^+)^{-1} \partial_x \eta \partial_x \xi + O(\mu). \quad (3.44)$$

Finally, we obtain the governing equations for  $\eta$  and  $\xi$  upon substituting these expansions into the kinematic and dynamic boundary conditions

$$\eta_t + u_x + (\eta u)_x - R[\mathcal{T}u + \mathcal{T}\eta u + \eta \mathcal{T}u + \eta \mathcal{T}(\eta u)]_x = 0, \quad (3.45)$$

$$u_t + (1 - R)\eta_x + uu_x - \tau \eta_{xxx} + \frac{E_b(1 - \varepsilon)^2}{\varepsilon} \mathcal{T}\eta_x - R[u\mathcal{T}u + u\mathcal{T}(\eta u)]_x = 0, \quad (3.46)$$

where the pseudo-differential operator  $\mathcal{T}$  is defined as

$$\mathcal{T} = \frac{(-\partial_{xx})^{1/2}}{\tanh(h(-\partial_{xx})^{1/2})}. \quad (3.47)$$

Note that the governing system (3.45) and (3.46) has been rewritten in a more revealing form via differentiating the dynamic boundary condition with respect to  $x$  and letting  $u = \xi_x$ .

A slightly different nonlinear model can be derived by using  $\xi^-$  instead of  $\xi$  as the unknown. Recalling the kinematic boundary condition (2.16) and the related operator expansions, one can express  $\xi^+$  as

$$\xi^+ = -(G^+)^{-1} \eta_t = -(G_0^+)^{-1} \eta_t + O(\mu). \quad (3.48)$$

Substituting (3.48) into the dynamic boundary condition (3.2) and retaining terms valid up to  $O(\mu)$ , one obtains

$$\xi_t^- + R(G_0^+)^{-1} \eta_{tt} + \frac{1}{2} (\xi_x^-)^2 + (1 - R)\eta + \frac{E_b(1 - \varepsilon)^2}{\varepsilon} \mathcal{T}\eta - \tau \eta_{xx} = 0. \quad (3.49)$$

The approximate kinematic boundary condition is constructed by the retention of terms up to  $O(\mu^2)$  in the expansion of  $G^-$ . One finally obtains

$$\eta_t + u_x + (\eta u)_x = 0, \quad (3.50)$$

$$u_t + (1 - R)\eta_x + uu_x + \frac{E_b(1 - \varepsilon)^2}{\varepsilon} \mathcal{T}\eta_x - \tau \eta_{xxx} + R\mathcal{T}[(1 + \eta)u]_t = 0, \quad (3.51)$$

where we have written  $u = \xi_x^-$  as before. The system (3.50) and (3.51) has an inbuilt advantage over the system (3.45) and (3.46) in computing solitary waves. To illustrate this, we assume that a solitary wave propagates with a constant speed  $c$ , and the wave becomes static in the moving frame  $X = x - ct$ . By integrating (3.50), one can show easily that  $u = c\eta/(1 + \eta)$ . After substituting this relation into (3.51), an integrodifferential equation for  $\eta$  is obtained:

$$-\frac{c^2 \eta(2 + \eta)}{2(1 + \eta)^2} + (1 - R)\eta + \left[ \frac{E_b(1 - \varepsilon)^2}{\varepsilon} - c^2 R \right] \mathcal{T}\eta - \tau \eta_{XX} = 0, \quad (3.52)$$

which can be solved by some numerical iteration method. However, (3.45) cannot relate  $\eta$  and  $u$  explicitly, complicating the problem.

### 3.3. Barannyk–Papageorgiou–Petropoulos scaling

Barannyk *et al.* (2012, 2015) considered the problem of interfacial electrocapillary-gravity waves between two perfect dielectrics under a horizontal electric field. To understand the effects of the electric field on the Rayleigh–Taylor instability, they proposed a nonlinear long-wave model based on novel scaling. Their scaling assumes that interfacial waves are long relative to the upper-layer thickness but of comparable length with the lower-layer thickness. More precisely, the scales are chosen as

$$\left. \begin{aligned} \partial_x = O(1), \quad \partial_t = O(\mu), \quad \eta = O(\mu^2), \quad \xi^+ = O(\mu), \quad h = O(\mu^2), \\ R = O(1), \quad \varepsilon = O(1), \quad E_b = O(1), \quad \tau = O(1). \end{aligned} \right\} \quad (3.53)$$

Under the Barannyk–Papageorgiou–Petropoulos scaling, the kinematic boundary condition (2.16) indicates that

$$\xi^- = -(G^-)^{-1}G^+\xi^+ = -(G_0^-)^{-1}(h|D|^2 + \partial_x\eta\partial_x)\xi^+ + O(\mu^5), \quad (3.54)$$

where  $G_0^- = |D| \tanh(|D|)$ . It follows directly that  $\xi^- = O(\mu^3)$ . One proceeds by expanding the pseudo-differential operators in powers of  $\mu$  in the boundary conditions at the interface, as before. Retaining terms valid up to  $O(\mu^3)$  for the kinematic boundary condition, and up to  $O(\mu^2)$  for the dynamic boundary condition, yields

$$\eta_t - h\xi_{xx}^+ + (\eta\xi_x^+)_x = 0, \quad (3.55)$$

$$\xi_t^+ + \frac{1}{2}(\xi_x^+)^2 + \frac{E_b(1-\varepsilon)^2}{R}(G_0^-)^{-1}\eta_{xx} - \frac{1-R}{R}\eta + \frac{\tau}{R}\eta_{xx} = 0. \quad (3.56)$$

Changing variables as

$$\eta = h(1 - \tilde{\eta}), \quad \xi_x^+ = \sqrt{h}u, \quad \partial_t = \sqrt{h}\partial_\tau, \quad (3.57a-c)$$

one arrives at the system

$$\tilde{\eta}_\tau + (u\tilde{\eta})_x = 0, \quad (3.58)$$

$$R(u_\tau + uu_x) - E_b(1-\varepsilon)^2(G_0^-)^{-1}\tilde{\eta}_{xxx} + (1-R)\tilde{\eta}_x - \tau\tilde{\eta}_{xxx} = 0, \quad (3.59)$$

which is the same as obtained by Barannyk *et al.* (2012). It is noted that, unlike the Benjamin equation, the dispersive effects in the system (3.58) and (3.59) come from only the electric field and surface tension. That is because the Barannyk–Papageorgiou–Petropoulos scaling gives rise to a very small  $\xi^-$ , which excludes the motion of the deep layer when truncating the asymptotic expansion at an appropriate order. Though there is a smallness assumption on wave amplitude, the system can be viewed as a strongly nonlinear model since the amplitude is of the same order as the upper-layer thickness. The system (3.58) and (3.59) demonstrates interesting dynamics, including suppressing the Rayleigh–Taylor instability, self-similar solutions, and touch-up singularities, and interested readers are referred to Barannyk *et al.* (2015) for more details.

### 4. Numerical calculations

This section presents the numerical scheme for solitary waves in the fully nonlinear problem (2.1a,b)–(2.7). We take a frame of reference moving with the solitary wave so that the flow is steady. Recalling  $W^\pm = V^\pm/E_0 - x$ , it is suitable to rescale the length, velocity potentials and perturbations of electric-field potentials by using  $h^-$ ,  $ch^-$  and  $h^-$ ,



respectively, where  $c$  is the translating speed of the solitary wave. The interface is assumed to be symmetric, with the  $y$ -axis the line of symmetry, and decay to zero in the far field. Therefore, the velocity becomes a unit as  $x \rightarrow \pm\infty$  in the new frame of reference.

#### 4.1. *Boundary integral equations*

Define the complex velocity potentials as

$$f^\pm(z) = \phi^\pm(z) + i\psi^\pm(z), \tag{4.1}$$

where  $\psi^\pm$  are stream functions as well as the complex conjugates of the corresponding velocity potentials, and  $z = x + iy$  stands for a point on the complex plane. Without loss of generality, we assume  $\phi^\pm = 0$  at  $x = 0$ , and  $\psi^\pm = 0$  at the interface. It follows from the non-dimensionalisation scheme that  $\psi^- = -1$  at the bottom, and  $\psi^+ = h$  at the top. Using a hodograph transformation that exchanges the independent and dependent variables, the lower (upper) layer is mapped conformally onto the infinite strip  $-1 < \psi^- < 0$  ( $0 < \psi^+ < h$ ) in the  $\phi^\pm + i\psi^\pm$  plane. The impermeability boundary conditions at two rigid walls can be satisfied automatically by using the method of images. Specifically, the function  $dz/df^+ - 1$  can be reflected in the line  $\psi^+ = h$  to produce a function analytic in  $0 < \psi^+ < 2h$ , and the same procedure can be applied to the lower-layer fluid and the analytic function  $dz/df^- - 1$ . Since the velocity potential is discontinuous across the interface, an auxiliary function  $\chi$  can be introduced such that  $\chi(\phi^-) = \phi^+$  at the interface. Hereafter, we use  $\phi^-$  as the primary independent variable and suppress its superscript for ease of notation. Applying the Cauchy integral formula to both lower- and upper-layer fluids results in the two integral equations

$$x_\phi(\phi_m) - 1 = \frac{1}{\pi} \int_{-\infty}^{\infty} \left[ \frac{2(x_\phi - 1) - y_\phi(\phi - \phi_m)}{(\phi - \phi_m)^2 + 4} - \frac{y_\phi}{\phi - \phi_m} \right] d\phi, \tag{4.2}$$

$$\frac{x_\phi}{\chi_\phi}(\phi_m) - 1 = \frac{1}{\pi} \int_{-\infty}^{\infty} \left[ \frac{2h(x_\phi - \chi_\phi) + y_\phi(\chi(\phi) - \chi(\phi_m))}{(\chi(\phi) - \chi(\phi_m))^2 + 4h^2} + \frac{y_\phi}{\chi(\phi) - \chi(\phi_m)} \right] d\phi, \tag{4.3}$$

where the functions  $x_\phi$  and  $y_\phi$  are evaluated at the interface, and both  $\phi$  and  $\phi_m$  represent the horizontal coordinate of the  $\phi^- + i\psi^-$  plane. For the electric field, we introduce the complex voltage potentials

$$q^\pm(z) = W^\pm(z) + iU^\pm(z), \tag{4.4}$$

where  $W^\pm$  are defined in § 2.1, and  $U^\pm$  are newly introduced complex conjugate functions. Based on the Cauchy integral formula, two integral equations are obtained:

$$W_\phi(\phi_m) = \frac{1}{\pi} \int_{-\infty}^{\infty} \left[ \frac{2W_\phi + U_\phi^-(\phi - \phi_m)}{(\phi - \phi_m)^2 + 4} + \frac{U_\phi^-}{\phi - \phi_m} \right] d\phi, \tag{4.5}$$

$$\frac{W_\phi}{\chi_\phi}(\phi_m) = \frac{1}{\pi} \int_{-\infty}^{\infty} \left[ \frac{2hW_\phi - U_\phi^+(\chi(\phi) - \chi(\phi_m))}{(\chi(\phi) - \chi(\phi_m))^2 + 4h^2} - \frac{U_\phi^+}{\chi(\phi) - \chi(\phi_m)} \right] d\phi, \tag{4.6}$$

where  $W$  stands for the perturbation of the voltage potential at the interface, as before. In the transformed plane, the continuity condition of the electric displacement field and the

dynamic boundary condition are recast to

$$(\varepsilon - 1)y_\phi = \varepsilon U_\phi^+ - U_\phi^-, \tag{4.7}$$

$$\begin{aligned} \frac{F^2}{2J} (1 - R\chi_\phi^2) + (1 - R) \left( y - \frac{F^2}{2} \right) + \frac{E_b}{2J} (U_\phi^{-2} - W_\phi^2) - \frac{\varepsilon E_b}{2J} (U_\phi^{+2} - W_\phi^2) \\ - \frac{E_b(1 - \varepsilon)}{J} x_\phi W_\phi - \frac{\tau}{J^{3/2}} (y_{\phi\phi} x_\phi - x_{\phi\phi} y_\phi) = 0, \end{aligned} \tag{4.8}$$

respectively, where  $J = x_\phi^2 + y_\phi^2$  is the Jacobian of the transformation, and  $F = c/\sqrt{gh^-}$  is the Froude number measuring the wave speed.

The problem being considered is as follows: given one of the two parameters  $H = y(0)$  and  $F$ , we seek solitary-wave solutions to the system (4.2), (4.3), (4.5)–(4.8). Since we confine our attention to symmetric solutions in the present paper, it is sufficient to perform numerical computations on a half real line (say,  $0 \leq \phi < \infty$ ). Due to the decaying nature of solitary waves, a truncated domain  $[0, L)$  with large  $L$  is used in numerical computations. We introduce a set of mesh grids

$$\phi_i = \frac{(i - 1)L}{N}, \quad i = 1, 2, \dots, N, \tag{4.9}$$

and the corresponding unknowns

$$\frac{dy}{d\phi}(\phi_i), \quad \frac{dx}{d\phi}(\phi_i), \quad \frac{d\chi}{d\phi}(\phi_i), \quad \frac{dW}{d\phi}(\phi_i), \quad \frac{dU^-}{d\phi}(\phi_i), \quad F; \tag{4.10}$$

$U_\phi^+$  can be obtained through (4.7). The symmetry of solutions gives

$$y_\phi(0) = 0, \quad U_\phi^-(0) = 0, \tag{4.11a,b}$$

and additionally, the decaying nature of solitary waves indicates that

$$x_\phi(\phi_N) = 1, \quad \chi_\phi(\phi_N) = 1, \quad W_\phi(\phi_N) = 0. \tag{4.12a-c}$$

Overall, there are  $5N - 4$  unknowns, and we need the same number of equations. To avoid the singularities in computations of the Cauchy integrals, we introduce another set of mesh grids

$$\phi_{i+1/2} = \frac{\phi_i + \phi_{i+1}}{2}, \quad i = 1, 2, \dots, N - 1. \tag{4.13}$$

Evaluating (4.2)–(4.6) and (4.8) at the midpoints  $\phi_{i+1/2}$  results in  $5N - 5$  algebraic equations. We can specify the wave displacement at the centre to close the system, namely  $\eta(0) = H$ . It is noted that this condition should be omitted while computing a solitary wave with a prescribed Froude number. Here,  $x$ ,  $y$  and  $\chi$  can be obtained by integrating their derivatives using the trapezoidal rule. The derivatives  $x_{\phi\phi}$  and  $y_{\phi\phi}$  are computed via the five-point centred difference scheme. And the unknowns at the midpoints are calculated by a fourth-order interpolation formula.

The fully nonlinear equations are solved via a Newton iteration method. The program is considered to have converged to a solution when the  $l^\infty$ -norm of the residual error is less than  $10^{-10}$ . The initial guess of the iteration is obtained by applying an artificial pressure to the interface and then eliminating it gradually via a numerical continuation. Once a solitary-wave solution is found, other solutions on the same branch are computed via a

straightforward continuation method by changing the Froude number, the wave amplitude or other parameters. Finally, the number of grid points is chosen sufficiently large ( $N \geq 2000$ ), and the grid spacing is chosen sufficiently small ( $L/N \leq 0.1$ ), to ensure accurate enough solutions.

#### 4.2. Results

Before presenting numerical results, it is necessary to discuss the condition for the existence of solitary waves from the viewpoint of linear theory. First, the linear dispersion relation in the dimensionless form reads

$$F^2 = \frac{\tanh(k) \tanh(kh)}{k[\tanh(kh) + R \tanh(k)]} \left[ 1 - R + \frac{E_b(1 - \varepsilon)^2 k}{\varepsilon \tanh(kh) + \tanh(k)} + \tau k^2 \right]. \quad (4.14)$$

Despite the nonlinear nature of solitary waves, the linear dispersion relation provides a necessary condition for their existence. Namely, the function  $F$  defined in (4.14) should have global extrema, where the group velocity and the phase velocity are equal. If the extremum occurs at  $k = 0$ , then solitary waves that can be described asymptotically by the KdV equation in the weakly nonlinear regime may exist (below the minimum or above the maximum). On the other hand, when the extreme occurs at a non-zero wavenumber, wavepacket solitary waves with damped oscillations can be expected. It is emphasised that, as discussed in the Introduction, searching for interfacial wavepacket solitary waves does not require a normal-form analysis unless one is concerned with the bifurcation mechanism of solitary waves in the vicinity of the bifurcation point, which is beyond the scope of this paper.

The classical dispersion relation of interfacial capillary-gravity waves in the absence of a horizontal electric field is shown in figure 2(a). The  $k$ - $F$  curves for a stable density stratification ( $R < 1$ ) are plotted for different values of interfacial tension. When the interfacial tension is neglected ( $\tau = 0$ ), the phase speed is a monotonically decreasing function of wavenumber, hence solitary waves may exist above the global maximum occurring at  $k = 0$ . As the interfacial tension increases, the dispersion curve first experiences a global minimum at a non-zero wavenumber and then becomes strictly increasing. As discussed before, solitary waves under these two situations are of different types if they exist.

Figure 2(b) shows the regularising effect of the horizontal electric field, which may support solitary waves even for an unstable density stratification of fluids ( $R > 1$ ). For  $R = 1.2$ , the  $k$ - $F^2$  curves are plotted with various values of electric strength. Without an electric field, waves are in the Rayleigh–Taylor unstable regime ( $F^2$  is negative for small wavenumbers), and no solitary waves are expected. However, a considerably large electric field can make  $F^2$  positive for all wavenumbers to suppress the Rayleigh–Taylor instability. The positivity of  $F$  indicates a global minimum occurring at either  $k = 0$  or  $k \neq 0$ , which may result in different types of solitary waves below the phase speed minimum. It is noted that a local extremum (see, for example, the circle in figure 2b) cannot support solitary waves due to a resonance between long and short waves, usually resulting in generalised solitary waves with non-decaying trains of ripples.

In the following subsections, we exhibit numerical results for three different regions of the density ratio:  $R > 1$ ,  $R = 1$  and  $R < 1$ . Besides the density ratio, the parameter space includes four other dimensionless parameters: the depth ratio  $h$ , the permittivity ratio  $\varepsilon$ , the electric strength  $E_b$ , and the surface tension  $\tau$ . We choose appropriate parameter sets to display new solitary-wave solutions under the electric field.

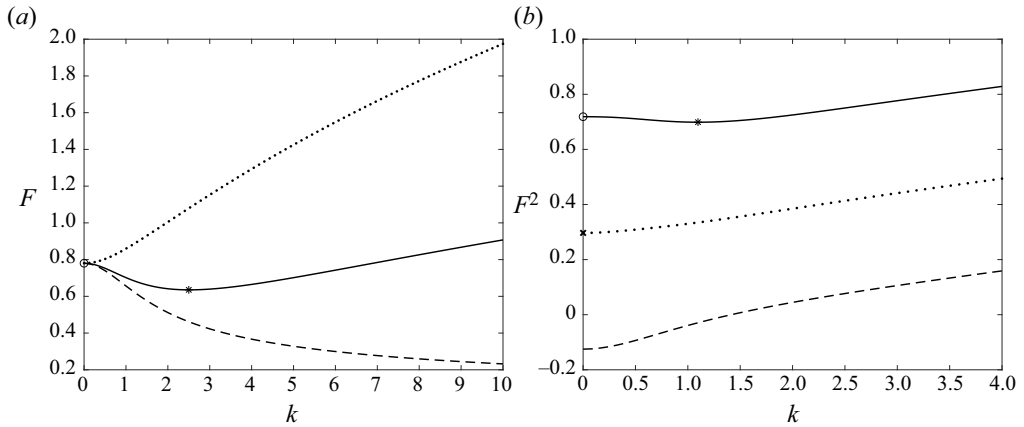


Figure 2. (a) Dispersion relations ( $k$ - $F$  curve) for interfacial capillary-gravity waves. The parameters are chosen as  $R = 0.3$ ,  $h = 2$ ,  $E_b = 0$ , with  $\tau = 0$  (dashed line),  $\tau = 0.1$  (solid line) and  $\tau = 0.5$  (dotted line). Symbols: circle,  $k = 0$  and  $F = 0.78$ ; asterisk,  $k = 2.514$  and  $F = 0.635$  (phase speed minimum). (b) Dispersion relations ( $k$ - $F^2$  curve) for interfacial electrocapillary-gravity waves for  $R = 1.2$ ,  $h = 2$ ,  $\varepsilon = 0.1$ ,  $\tau = 0.1$ , with  $E_b = 0$  (dashed line),  $E_b = 1$  (dotted line), and  $E_b = 2$  (solid line). Symbols: cross,  $k = 0$  and  $F^2 = 0.297$ ; circle,  $k = 0$  and  $F^2 = 0.719$ ; asterisk,  $k = 1.097$  and  $F^2 = 0.699$  (phase speed minimum).

#### 4.2.1. $R > 1$

This regime can be explored due entirely to the horizontal electric field, which regularises the Rayleigh–Taylor instability. We first use the following parameters:  $R = 1.5$ ,  $h = 2$ ,  $\varepsilon = 2$ ,  $E_b = 3$  and  $\tau = 0.3$ . The dispersion relation shown in figure 3(a) has a global minimum at  $k = 0$ . Therefore, solitary waves may exist below this minimum and can be approximated asymptotically by the sech-squared solutions of the KdV equation (3.15) when the wave amplitude is small. The free-surface displacement at the centre,  $\eta(0)$ , is plotted versus the dimensionless wave speed,  $F$ , in figure 3(b), and a typical wave profile ( $F = 0.2216$ ) is shown in figure 3(c). The comparison between the numerical results from the electrified Euler equations (solid line) and the theoretical prediction of the KdV equation (dotted line) shows good agreement for small- and moderate-amplitude solitary waves. In a certain respect, it confirms the effectiveness of the weakly nonlinear theory and the correctness of the numerical algorithm of the fully nonlinear equations. We vary the wave speed to complete the bifurcation diagram, and terminate the computation when the trough of the solitary wave almost touches the bottom boundary. Figure 3(d) shows the typical profiles of large-amplitude solitary waves. The solid curve is the solution of the largest amplitude that we can obtain, which has developed a remarkable, almost touch-down configuration ( $\eta(0) = -0.9999$ , recalling that the thickness of the lower layer was non-dimensionalised to unity in the beginning). Touch-up/down singularities are common nonlinear interfacial phenomena in electrohydrodynamic instabilities, which are confirmed by laboratory experiments and numerical simulations (see, for example, Papageorgiou 2019) and have wide applications in microscale technologies, such as the sub-micrometre replication techniques in integrated circuits (Schäffer *et al.* 2000). In this example, the curvature (or, equivalently, the second derivative of  $y$ ) singularity occurs when approaching the limiting configuration (i.e. bounded interfacial gradient but unbounded curvature; see the enlarged view of the wave trough in figure 3d), akin to the touch-up instability of interfacial electrohydrodynamic waves shown by Barannyk *et al.* (2015).

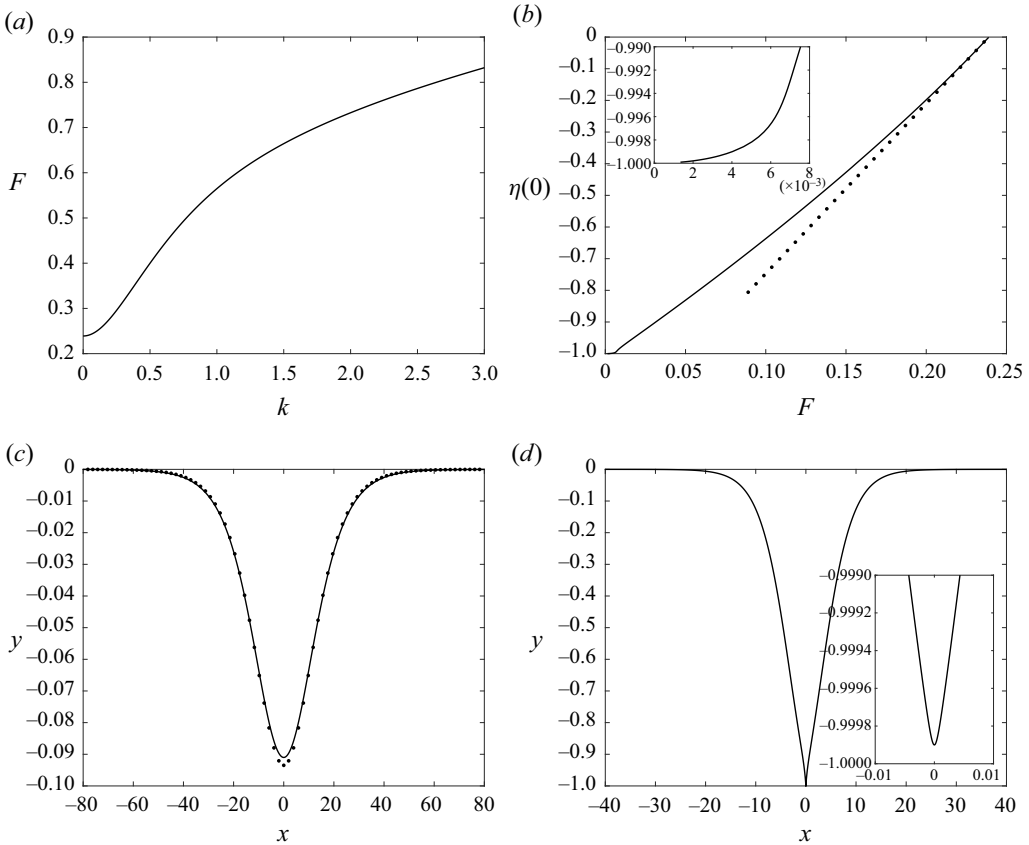


Figure 3. (a) Dispersion relation when a strong electric field regularises the Rayleigh–Taylor instability; parameters are chosen as  $R = 1.5$ ,  $h = 2$ ,  $\varepsilon = 2$ ,  $E_b = 3$  and  $\tau = 0.3$ . (b) Speed–amplitude bifurcation curves of solitary waves for the electrified Euler equations (solid line) and the KdV equation (dots). The curve near the limiting point ( $F = 0$  and  $\eta(0) = -1$ ) is shown in detail. (c) Solutions of the Euler equations (solid line) and the KdV equation (dotted line) for  $F = 0.22$ . (d) Typical profiles for the almost touch-down configuration with  $\eta(0) = -0.9999$ .

The dispersion relation may have two local minima competing for the global minimum. A typical example is shown in figure 4(a) with  $R = 1.1$ ,  $h = 2$ ,  $\varepsilon = 0.2$ ,  $E_b = 3.5$  and  $\tau = 0.1$ . Two local minima occur at  $k = 0$  and  $k = 1.269$ , and the latter one possesses the smaller value of  $F$  and hence the global minimum. As a consequence, wavepacket solitary waves are expected. The speed–amplitude bifurcation curves and typical wave profiles are displayed in figures 4(b) and 4(c), respectively. Two fundamental branches are found in this type of solitary wave, including one family of waves with a positive displacement at their centre – denoted waves of elevation – and another family of waves with a negative displacement at their centre – denoted waves of depression. Both branches bifurcate from infinitesimal periodic waves at the minimum of the phase speed ( $F = 0.977$ ). The elevation wave is a single-hump solution, and the depression wave features two humps placed side-by-side. We trace the bifurcation curve by varying the wave speed, and terminate the numerical program when Newton’s method oscillates and fails to reach the desired accuracy (presumably since the wave crest becomes sharp and further increasing amplitude is sensitive to perturbations).

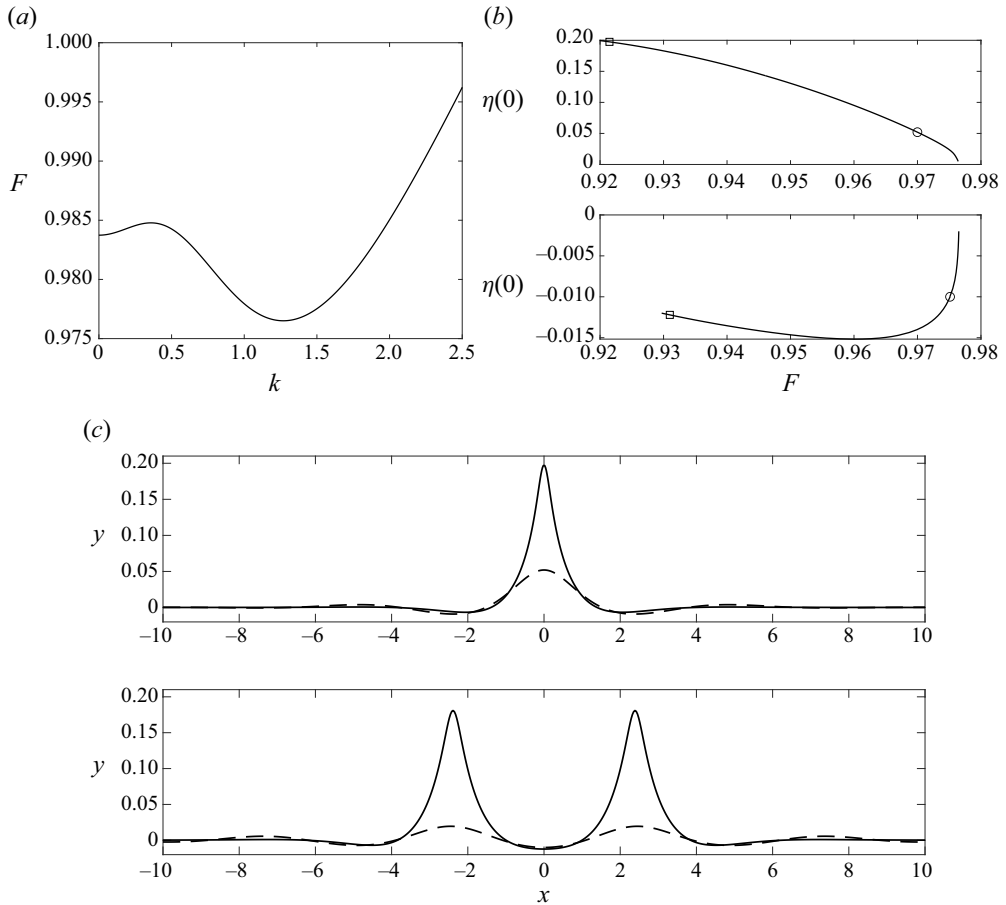


Figure 4. (a) Dispersion relation for  $R = 1.1$ ,  $h = 2$ ,  $\varepsilon = 0.2$ ,  $E_b = 3.5$  and  $\tau = 0.1$ , which has a global minimum  $F = 0.977$  at  $k = 1.269$ . (b) Speed–amplitude bifurcation curves of the elevation branch (top) and depression branch (bottom). (c) Typical wave profiles of elevation type (top) and depression type (bottom). Dashed lines and solid lines correspond to circles and squares in (b).

The other case is shown in [figure 5](#), where the long-wave phase speed is smaller than the local minimum at the non-zero wavenumber, which gives the phase speed minimum  $F = 0.8893$  at  $k = 0$ . The bifurcation curve (wave speed versus wave displacement at the centre) shown in [figure 5\(b\)](#) has a turning point near the global minimum of  $F$ . The corresponding wave profile is displayed in the middle of [figure 5\(c\)](#), which features monotonic decay on either side of the wave crest. Away from the turning point, solutions are characterised by a train of small-amplitude oscillations riding on the crest of a solitary wave of KdV type (see the second and fourth figures in [figure 5\(c\)](#)). They are akin to free-surface parasitic capillary waves, which can be viewed as a perturbation due to the effect of surface tension on a progressive pure gravity wave. This new type of solitary wave may be attributed largely to the local minimum of the phase speed at  $k = 1.269$  which is very close to the global minimum and therefore exerts a considerable impact on the waveform through wave interactions. Surprisingly, in this case, the solution branch does not bifurcate from the global phase speed minimum, and solitary waves can exist only

*Interfacial electrohydrodynamic solitary waves*

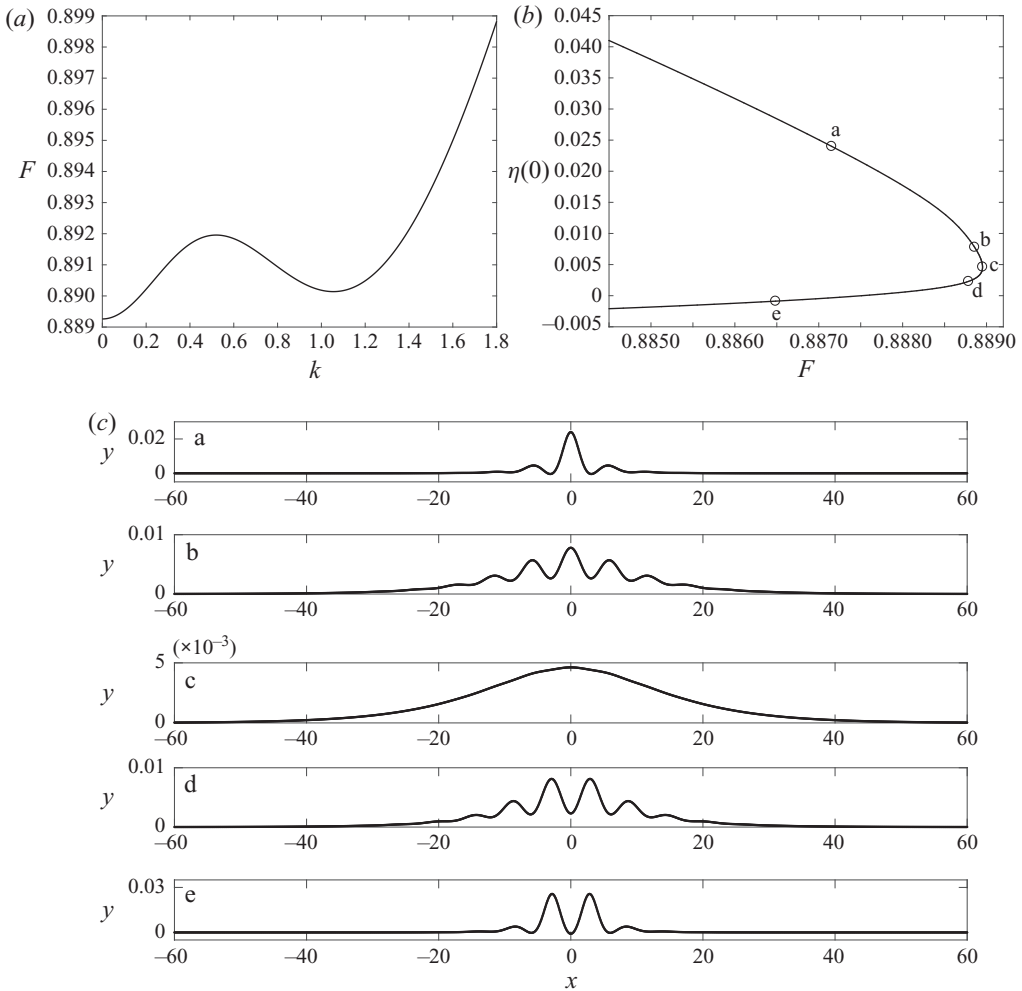


Figure 5. (a) Dispersion relations for  $E_b = 2.9$ ,  $R = 1.1$ ,  $h = 2$ ,  $\varepsilon = 0.2$  and  $\tau = 0.1$ . (b) Speed–amplitude bifurcation curve near the phase speed minimum. (c) Typical profiles corresponding to the circles in (b), from top to bottom.

at finite amplitude (see figure 5(b) and notice that the maximum value of  $|\eta|$  is always positive even when  $\eta(0) = 0$ ).

There is one particular situation in which the global minimum of the phase speed is attained at both  $k = 0$  and  $k \neq 0$  simultaneously. We choose  $R = 1.1$ ,  $h = 2$ ,  $\varepsilon = 0.2$ ,  $\tau = 0.1$  and  $E_b = 2.966$ . In this case, the global phase speed minimum ( $F = 0.90014$ ) occurs at  $k = 0$  and  $k = 1.086$ . Typical wave profiles are shown in figure 6, where the dashed lines highlight the wave envelopes in the modulational regime. Due to the apparent up–down asymmetry of wave envelopes, these solutions are neither the KdV-soliton type nor the wavepacket type. Such an exotic wave phenomenon arises due to the complicated dispersion relation resulting in long- and short-wave interactions. Indeed, it merits careful study from the asymptotic point of view, which is left for future work.

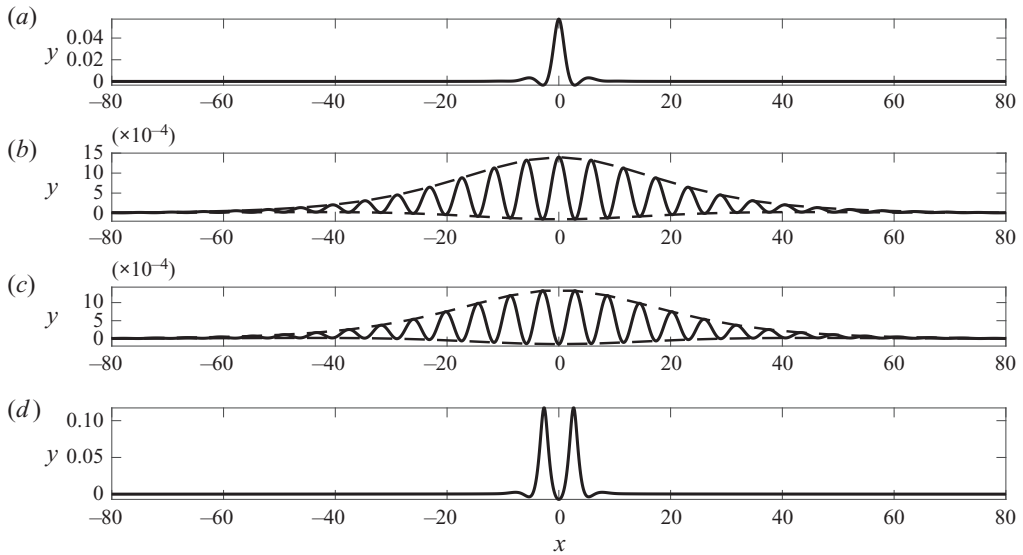


Figure 6. Typical profiles of KdV-wavepacket mixed type solitary waves with  $E_b = 2.966$ ,  $R = 1.1$ ,  $h = 2$ ,  $\varepsilon = 0.2$  and  $\tau = 0.1$ .

#### 4.2.2. $R = 1$

In the absence of the electric field, it is easy to know that solitary waves cannot exist in pure interfacial capillary waves (i.e.  $R = 1$ ) since the global minimum of the dispersion relation is  $F = 0$  and there is no global maximum. The situation will change if one considers the interfacial electrocapillary waves. In figure 7, we show examples with  $R = 1$ ,  $h = 1$ ,  $\varepsilon = 0.8$ ,  $E_b = 0.3$  and different values of  $\tau$ . For  $\tau = 0.1, 0.5$  and  $1.0$ , all dispersion relations attain the same global minimum ( $F = 0.0577$ ) at  $k = 0$  since the surface tension effect has no contribution to the long-wave speed. Elevation solitary waves are found to bifurcation from the phase minimum and exist for all positive  $F$  below. The wave amplitude keeps growing as  $F$  decreases, and ultimately, the wall touch-up phenomenon and the curvature singularity occur when approaching the limiting configuration near  $F = 0$ . An interesting feature, in this case, is that despite different wave profiles for a fixed wave amplitude (see figure 7c), they have the same speed. Hence, as displayed in figure 7(b), the speed–amplitude bifurcation curves with varying values of  $\tau$  coincide. This can be understood intuitively from the KdV equation (3.15) and its solution (3.18) in the weakly nonlinear regime, since the ratio of amplitude to speed depends only on  $\beta$ , which is independent of  $\tau$ . However, the coincidence for fully nonlinear solutions is challenging to elucidate due to the non-local nature of the electrified Euler equations.

Solutions are of particular interest when  $R = 1$  and  $\tau = 0$ ; that is, the horizontal electric field provides the only restoring force for the fluid system. In addition, we set  $h = 2$ ,  $\varepsilon = 0.2$ ,  $E_b = 0.5$ , and display the numerical results in figure 8. The dispersion relation is plotted in figure 8(a), where a global maximum of the dispersion relation appears at  $k = 0$ , and a branch of depression solitary waves is found for  $F > 0.39036$ . The speed–amplitude bifurcation curve is shown in figure 8(b), which features a ‘snake-like’ behaviour with several turning points. Starting from the phase speed maximum, we trace the curve by using the amplitude or speed interchangeably as the bifurcation parameter to traverse very sharp turning points or stationary points, respectively. After passing through two turning points near A and B, whose profiles are plotted in figure 8(c), a local bulge appears in



## Interfacial electrohydrodynamic solitary waves

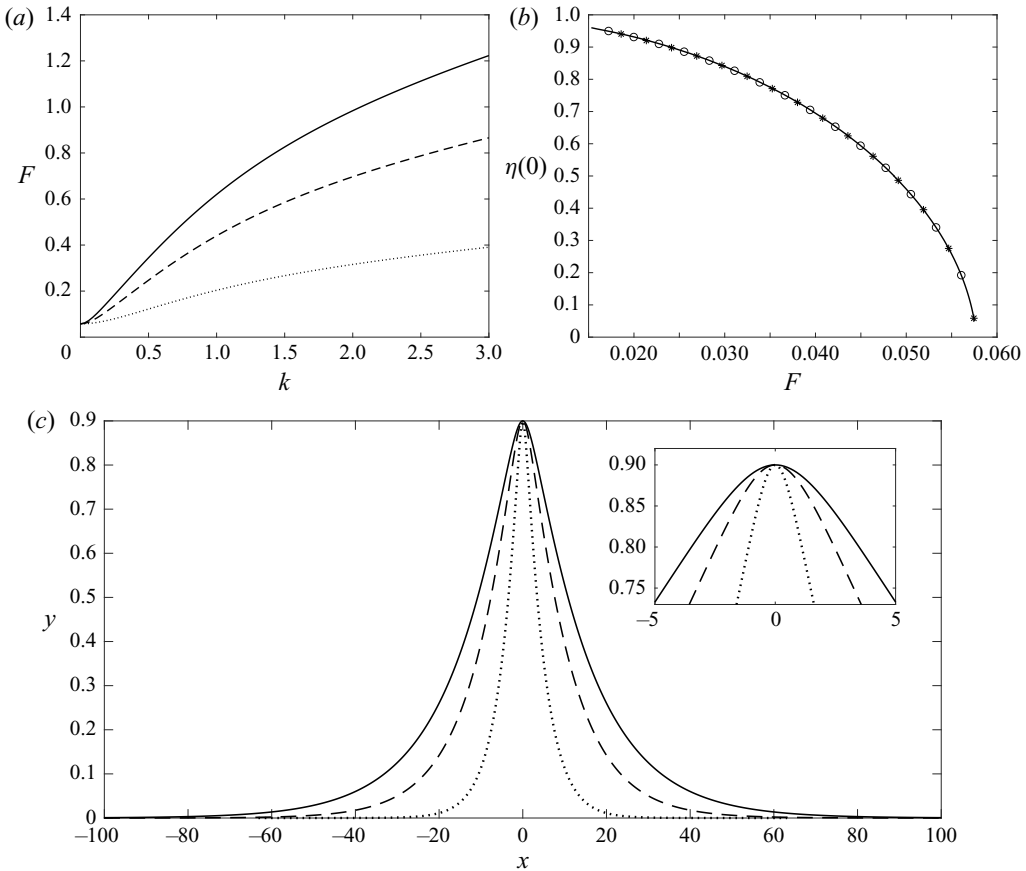


Figure 7. (a) Dispersion relations as  $\tau$  varies:  $\tau = 0.1$  (dotted line),  $\tau = 0.5$  (dashed line) and  $\tau = 1.0$  (solid line); other parameters are  $R = 1$ ,  $h = 1$ ,  $\varepsilon = 0.8$  and  $E_b = 0.3$ . (b) Speed–amplitude bifurcation curves:  $\tau = 0.1$  (solid line),  $\tau = 0.5$  (circles) and  $\tau = 1.0$  (asterisks). (c) Wave profiles for a fixed amplitude ( $\eta(0) = 0.9$ ) and variable  $\tau$ . The line styles are the same as those shown in (a).

the middle portion of the wave, and the solution is no longer similar to the sech-squared soliton. As we trace the bifurcation curve further, the bulge rises and expands, and  $\eta(0)$  gradually approaches zero. The interface becomes two fundamental depression waves placed side-by-side (see F of figure 8c).

### 4.2.3. $R < 1$

When the surface tension is sufficiently strong such that the global minimum of the dispersion relation is achieved at  $k = 0$ , the Benjamin equation (3.37) and the strongly nonlinear model (3.50) and (3.51) can provide good approximations for various nonlinear interfacial phenomena if the depth ratio satisfies  $h \gg 1$ . We still focus on solitary waves and compare numerical results of the reduced models against computations of the electrified Euler equations. The numerical scheme for constructing solitary-wave solutions in the reduced models is an extension of Petviashvili's method. The basic idea is to perform the iteration in the Fourier space supplemented by a normalisation factor (see Petviashvili (1976) and Wang (2017), for example). Following this idea, (3.52) can be written in the

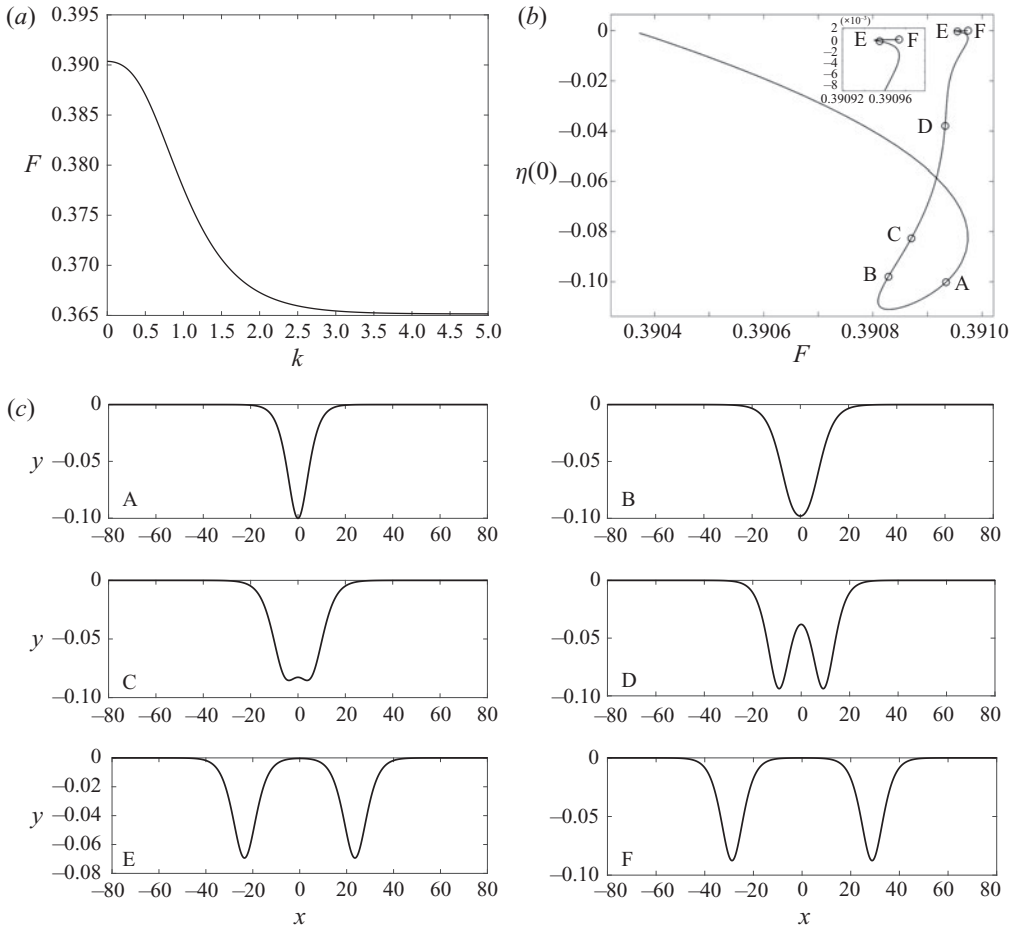


Figure 8. (a) Dispersion relations for pure electrified waves with  $R = 1$ ,  $\tau = 0$ ,  $h = 2$ ,  $\varepsilon = 0.2$  and  $E_b = 0.5$ . (b) ‘Snake-like’ bifurcation curve. The branch near points E and F is shown in detail. (c) Wave profiles corresponding to points A to F.

Fourier space as

$$\hat{\eta} = \frac{c^2 \widehat{\eta(2 + \eta)}}{2(1 + \eta)^2} = \mathcal{Q}[\hat{\eta}], \quad (4.15)$$

$1 - R + [E_b(1 - \varepsilon)^2/\varepsilon - c^2R]k/\tanh(hk) + \tau k^2$

where the hat symbol denotes the Fourier transform. To prevent the amplitude from going to zero or infinity, we need to introduce a multiplier in every iteration step, thus the numerical scheme can be proposed as

$$\hat{\eta}_{n+1} = (\alpha_n)^m \mathcal{Q}[\hat{\eta}_n] \quad \text{with } \alpha_n = \frac{\int |\hat{\eta}_n|^2 dk}{\int \hat{\eta}_n^* \mathcal{Q}[\hat{\eta}_n] dk}, \quad (4.16)$$

where the asterisk indicates complex conjugation, and  $m$  is a free parameter that needs to be chosen for convergence of the sequence  $\{\hat{\eta}_n\}$ . We found empirically that the iteration

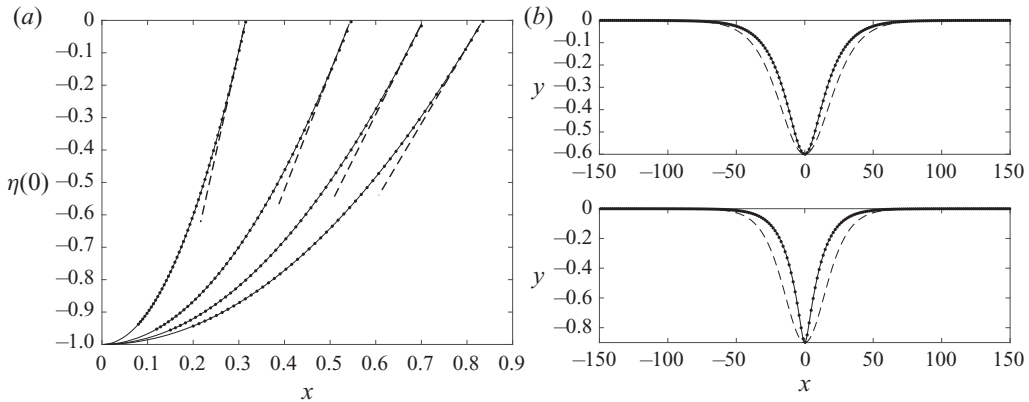


Figure 9. (a) Speed–amplitude bifurcation curves as  $R$  varies,  $R = 0.9, 0.7, 0.5$  and  $0.3$  (from left to right); other parameters are  $h = 50, \varepsilon = 0.8, E_b = 1$  and  $\tau = 10$ . Solutions are obtained with different models: the electrified Euler equations (solid lines), the Benjamin equation (dashed lines), and the strongly nonlinear equation (3.52) (dotted lines). (b) Comparisons of typical wave profiles for  $R = 0.9$ :  $\eta(0) = -0.6$  (top) and  $\eta(0) = -0.9$  (bottom). The line styles are the same as those in (a).

method (4.16) converges for  $1 \leq m \leq 2$ . The iteration scheme for the weakly nonlinear model (3.37) can be derived in the same vein, and we omit the detailed expressions.

We set  $h = 50, \varepsilon = 0.8, E_b = 1, \tau = 10$ , and vary  $R$  to obtain different solution branches. Single-trough depression solitary waves can be found for all values of  $R$  that we tested, and speed–amplitude bifurcation curves are plotted in figure 9(a). The Benjamin equation generally gives good predictions for small- and moderate-amplitude solitary waves; however, the strongly nonlinear model shows excellent agreement even when wave profiles almost touch the bottom (see comparisons of the waveform in figure 9b). We push the solution to the limiting configuration in computations of the full Euler equations. It is found again that the touch-down phenomenon and curvature singularity occur while approaching the static state, regardless of the density ratio.

Interfacial gravity solitary waves (without capillarity and electric field) were investigated extensively by different groups in the past few decades. One of the most striking findings is the broadening of the solitary pulse; that is, the midsection of the interface develops a plateau that becomes infinitely long when the wave speed approaches a limiting value (see the numerical computation by Turner & Vanden-Broeck (1988)). We attempt to learn the modification of the electric field on the broadening phenomenon. We first choose  $R = 0.997, h = 2, \varepsilon = 0.7, E_b = 0.5$  and  $\tau = 0$ , and this set of parameters yields a global maximum  $F = 0.1215$  at  $k = 0.6274$  (see figure 10a). Both elevation and depression branches of wavepacket solitary waves are found to bifurcate from this maximum, and wave profiles of moderate amplitude (dashed lines in figure 10c) are similar to those shown in figure 4. We draw the global bifurcation diagrams by varying the wave speed, and the wave crests start to become broad apparently as  $F > 0.1245$ . In contrast to the case without an electric field, the depression wave develops two plateaus during broadening (the bottom part of figure 10c). As shown by solid lines in figure 10(d), the connection between the two stays fixed, and either plateau expands in one direction only. The limiting profiles of the two branches have the same wave height ( $\approx 0.3869$ ) and the same wave speed ( $\approx 0.1249$ ). Close to the limiting point, the elevation and depression profiles overlap except for the middle hollow in the depression wave (see the comparison in figure 10d).

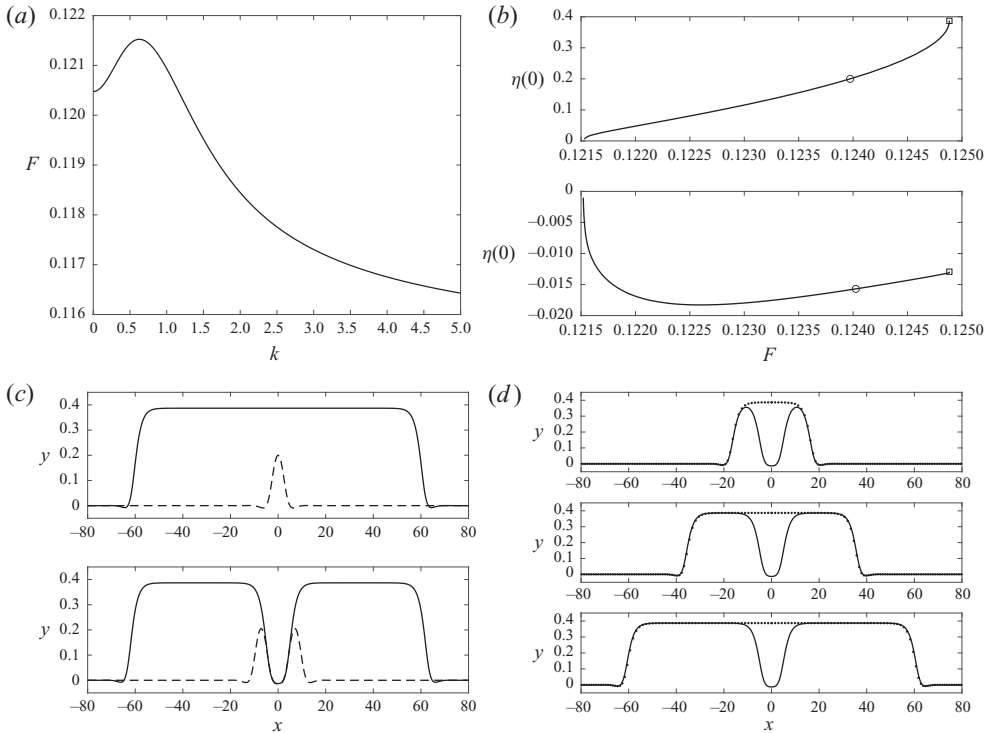


Figure 10. (a) Dispersion relation with  $R = 0.997$ ,  $h = 2$ ,  $\varepsilon = 0.7$ ,  $E_b = 0.5$  and  $\tau = 0$ . (b) Bifurcation curves of the elevation (top) and depression (bottom) branches parametrised by the value at the middle points of the waves. (c) Wave profiles corresponding to the solutions labelled by circles (dashed lines) and squares (solid lines) in (b). (d) Comparisons between elevation waves (dots) and depression waves (solid lines) near the limiting point.

As the broadening phenomenon occurs, the electric field may excite oscillations on the solitary pulse. Typical examples can be obtained when the global extremum of the phase speed is achieved at  $k = 0$ . We present results in figure 11 with  $R = 0.99$ ,  $h = 2$ ,  $\varepsilon = 0.2$ ,  $E_b = 5$  and  $\tau = 0$ . Via using  $F$  and  $\eta(0)$  alternately as the bifurcation parameter, the speed–amplitude (parametrised by the value at the middle point) diagram can be drawn, which features a helix-shaped behaviour with many turning points. Starting from the phase speed maximum and tracing the bifurcation curve, the KdV-type solitary wave becomes broader and broader by adding more and more oscillations on the midsection of the solitary wave.

### 5. Concluding remarks

In the present paper, nonlinear electrohydrodynamic interfacial waves propagating through the deformation of the interface between two superimposed layers of dielectric fluid under horizontal electric fields have been investigated from asymptotic and numerical perspectives. The electrified Euler equations have been reconstructed as the Zakharov–Craig–Sulem formulation through the extension of the Dirichlet–Neumann operator to the electric field. Consequently, a systematic procedure has been proposed to derive multi-scale models with weak or strong nonlinearity in various asymptotic limits. All the reduced models obtained here have Hamiltonian structures. This fact

*Interfacial electrohydrodynamic solitary waves*

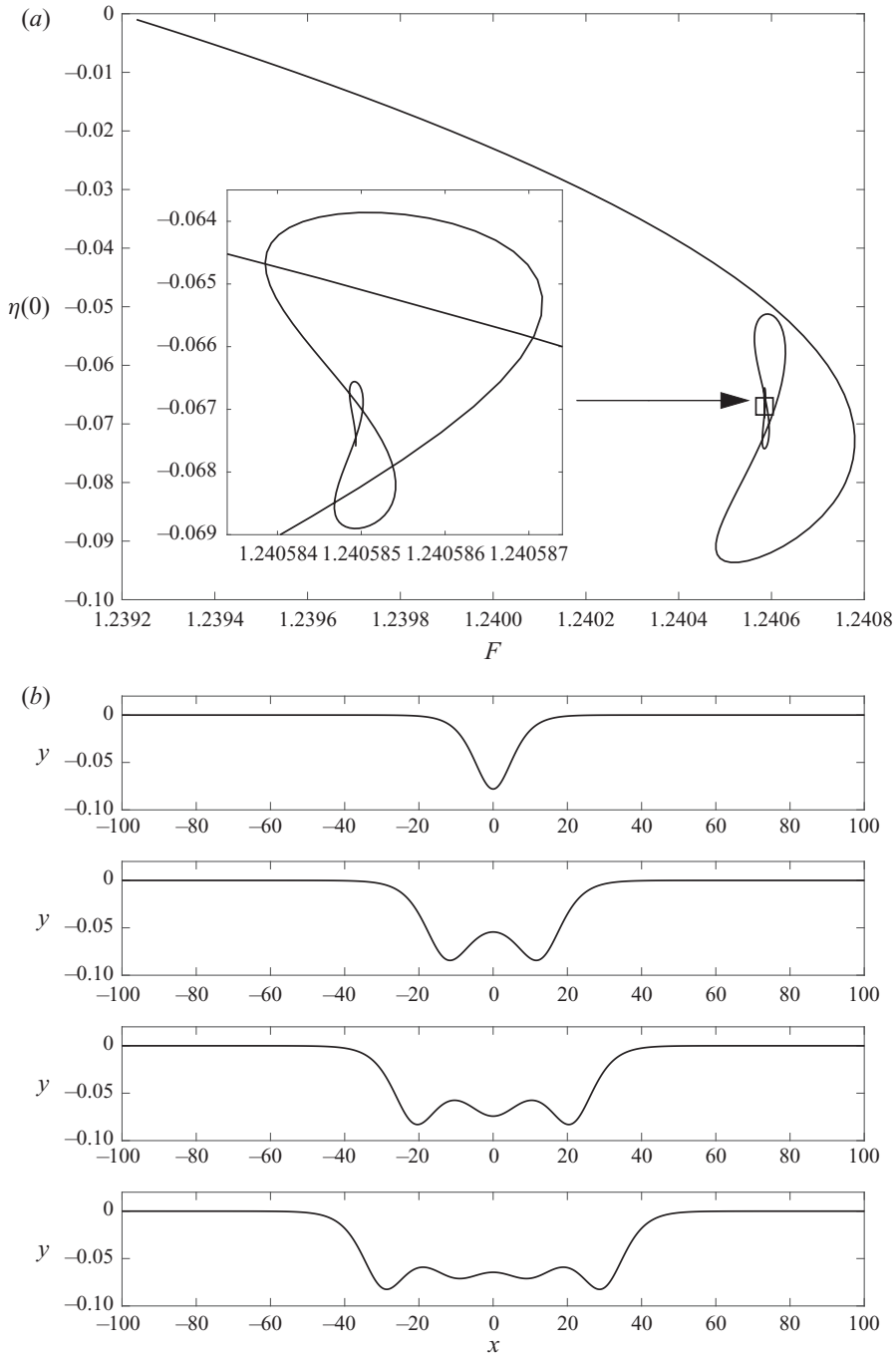


Figure 11. (a) ‘Snake-like’ bifurcation curve parametrised by the value at the middle point of waves with  $R = 0.99$ ,  $h = 2$ ,  $\varepsilon = 0.2$ ,  $E_b = 5$  and  $\tau = 0$ . The helix part is shown in detail in the inset. (b) Wave profiles with one to four troughs, from top to bottom.

is not only evident for weakly nonlinear models, such as the Boussinesq-type system, the KdV equation and its variants, and the Benjamin-type equation, but also valid for strongly nonlinear models. For example, the evolution equations (3.45) and (3.46) form a Hamiltonian system with the functional

$$\mathcal{H}[\eta, \xi] = \frac{1}{2} \int [(1 + \eta)\xi_x^2 + R(\xi \mathcal{T} \partial_x \eta \partial_x \xi + \xi \partial_x \eta \mathcal{T} \eta \partial_x \xi + \xi \mathcal{T} \partial_{xx} \xi + \xi \partial_x \eta \partial_x \mathcal{T} \xi)] dx + \frac{E_b(1 - \varepsilon)^2}{2\varepsilon} \int \eta_x (G_0^+)^{-1} \eta_x dx + \frac{1 - R}{2} \int \eta^2 dx + \frac{\tau}{2} \int \eta_x^2 dx, \tag{5.1}$$

and  $\eta$  and  $\xi$  are the canonical variables satisfying Hamilton's equations

$$\eta_t = \frac{\delta \mathcal{H}}{\delta \xi}, \quad \xi_t = -\frac{\delta \mathcal{H}}{\delta \eta}, \tag{5.2a,b}$$

where the right-hand sides represent the variational derivatives. In the same manner, the Barannyk–Papageorgiou–Petropoulos system (3.55) and (3.56) has the Hamiltonian

$$\mathcal{H}[\eta, \xi^+] = \frac{1}{2} \int \left[ (\eta - h)(\xi_x^+)^2 - \frac{E_b(1 - \varepsilon)^2}{R} \eta_x (G_0^-)^{-1} \eta_x - \frac{1 - R}{R} \eta^2 - \frac{\tau}{R} \eta_x^2 \right] dx. \tag{5.3}$$

It is also possible to write the electrified Euler equations in the Hamiltonian form. However, the proof is a bit mathematically involved, and the related work will be reported elsewhere in the near future.

These multi-scale models provide good approximations and theoretical underpinnings for small- and moderate-amplitude solutions in various asymptotic regimes. However, it is still necessary to seek solutions in the primitive equations to understand fully nonlinear wave phenomena such as the global bifurcation and limiting configurations of travelling waves. A numerical algorithm based on the modified boundary integral equation method has been developed to compute solitary waves in the full Euler equations coupled with electric effects. It has been found that the electric field has a significant impact on the physics system being investigated, and can change the qualitative nature of solitary interfacial waves from three perspectives. First, the regularising effect arising from the horizontal electric field expands the range of parameters for the existence of progressive waves; notably, the density ratios  $R > 1$  and  $R = 1$  may support solitary waves. Second, the electric field can change the qualitative characteristics of solitary waves; for instance, the infinite bilateral broadening of an interfacial gravity solitary pulse may be replaced by two abreast plateaus with unilateral expansion under the combined effect of gravity and electric field. Third, the coexistence of gravity, surface tension and electric forces may lead to a complicated dispersion relation giving rise to a new type of travelling waves, namely the KdV–wavepacket mixed type solitary waves.

Our theoretical and numerical results raise other questions. The first question is the stability of these solitary waves in the electrified Euler equations. For the present, a helpful quantity that can be checked is the velocity jump across the interface. It is found that a tangential velocity discontinuity exists in the pulse region for all solitary waves that we tested, and the system can therefore be susceptible to a Kelvin–Helmholtz instability. In order to put this intuition on a firm footing, a thorough linear stability analysis is needed. More importantly, since a horizontal electric field can regularise the system from the linear point of view, it is natural to ask whether and how it plays a role in the stability properties of nonlinear waves. Thus a numerical scheme for unsteady simulations is required to

understand the time evolution of a perturbed solitary wave. A possible scheme is to generalise the vortex sheet method pioneered by Baker, Meiron & Orszag (1982) to include electric effects. And this can be achieved by introducing another Birkhoff–Rott integral accounting for the electric field.

To further understand the bifurcation mechanism of wavepacket solitary waves, the nonlinear Schrödinger (NLS) equation is needed since it would tell us when to expect small-amplitude solitary-wave bifurcations from extrema of dispersion relations. When the NLS equation is defocusing at the extremum, wavepacket solitary waves usually appear along a branch of generalised solitary waves and exist at finite amplitude; a typical example is progressive hydroelastic waves in deep water (see Milewski, Vanden-Broeck & Wang (2011) for details). However, in this case, a numerical algorithm handling periodic waves in the electrified Euler equations is required in considering the computation of generalised solitary waves, which we leave for a future study. On the other hand, when the global extremum of the dispersion relation occurs at two different wavenumbers simultaneously, the bifurcation mechanism of the newly discovered solitary waves in this paper cannot be described by a single NLS equation. It is a particular case of the long–short wave interaction (see, for example, Benney 1977) and merits a thorough investigation. In addition, it is also of great interest to seek KdV–wavepacket mixed type solutions in other nonlinear wave systems.

Finally, the asymptotic procedure presented in the paper can be generalised easily to the three-dimensional problem. However, a horizontal electric field has a preferred direction and leads to an anisotropic dispersion relation in the three-dimensional case. Namely, it cannot provide a stabilising effect for linear waves propagating orthogonal to the electric field. It is of particular interest to find a way to regularise various interfacial instabilities (Kelvin–Helmholtz, Rayleigh–Taylor, etc.) in all horizontal directions.

**Acknowledgements.** The authors would like to thank Dr T. Gao (University of Greenwich) for very helpful discussions on matters relating to this article.

**Declaration of interests.** The authors report no conflict of interest.

**Funding.** This work was supported by the Key Program of the National Natural Science Foundation of China under grant 12132018, and the Strategic Priority Research Program of the Chinese Academy of Sciences under grant XDB22040203. X.G. would also like to acknowledge support from the Chinese Scholarship Council.

#### **Author ORCIDs.**

 Zhan Wang <https://orcid.org/0000-0003-4393-2118>.

#### REFERENCES

- AKYLAS, T.R. 1993 Envelope solitons with stationary crests. *Phys. Fluids* **5**, 789–791.
- ANDERSON, T.G., CIMPEANU, R., PAPAGEORGIOU, D.T. & PETROPOULOS, P.G. 2017 Electric field stabilization of viscous liquid layers coating the underside of a surface. *Phys. Rev. Fluids* **2**, 054001.
- BAKER, G.R., MEIRON, D.I. & ORSZAG, S.A. 1982 Generalized vortex methods for free-surface flow problems. *J. Fluid Mech.* **123**, 477–501.
- BARANNYK, L.L., PAPAGEORGIOU, D.T. & PETROPOULOS, P.G. 2012 Suppression of Rayleigh–Taylor instability using electric fields. *Maths Comput. Simul.* **82**, 1008–1016.
- BARANNYK, L.L., PAPAGEORGIOU, D.T., PETROPOULOS, P.G. & VANDEN-BROECK, J.-M. 2015 Nonlinear dynamics and wall touch-up in unstably stratified multilayer flows in horizontal channels under the action of electric fields. *SIAM J. Appl. Maths* **75** (1), 92–113.
- BENJAMIN, T.B. 1992 A new kind of solitary wave. *J. Fluid Mech.* **245**, 401–411.
- BENNEY, D.J. 1977 A general theory for interactions between short and long waves. *Stud. Appl. Maths* **56** (1), 81–94.
- CIMPEANU, R., PAPAGEORGIOU, D.T. & PETROPOULOS, P.G. 2014 On the control and suppression of the Rayleigh–Taylor instability using electric fields. *Phys. Fluids* **26**, 022105.

- COIFMAN, R. & MEYER, Y. 1985 Nonlinear harmonic analysis and analytic dependence. *Proc. Symp. Pure Math.* **43**, 71–78.
- CRAIG, W. & SULEM, C. 1993 Numerical simulation of gravity waves. *J. Comput. Phys.* **108**, 73–83.
- EASWARAN, C.V. 1988 Solitary waves on a conducting fluid layer. *Phys. Fluids* **31**, 3442–3443.
- ELDABE, N.T. 1989 Effect of a tangential electric field on Rayleigh–Taylor instability. *J. Phys. Soc. Japan* **58**, 115–120.
- FERNANDEZ DE LA MORA, J. & LOSCERTALES, I.G. 1994 The current emitted by highly conducting Taylor cones. *J. Fluid Mech.* **260**, 155–184.
- GAMERO-CASTAÑO, M. & HRUBY, V. 2001 Electro spray as a source of nanoparticles for efficient colloid thrusters. *J. Propul. Power* **17** (5), 977–987.
- GAO, T., MILEWSKI, P.A., PAPAGEORGIU, D.T. & VANDEN-BROECK, J.-M. 2017 Dynamics of fully nonlinear capillary-gravity solitary waves under normal electric fields. *J. Engng Maths* **108**, 107–122.
- GLEESON, H., HAMMERTON, P., PAPAGEORGIU, D.T. & VANDEN-BROECK, J.-M. 2007 A new application of the Kortweg–de Vries Benjamin–Ono equation in interfacial electrohydrodynamics. *Phys. Fluids* **19**, 031703.
- GRANDISON, S., PAPAGEORGIU, D.T. & VANDEN-BROECK, J.-M. 2007 Interfacial capillary waves in the presence of electric fields. *Euro. J. Mech. (B/Fluids)* **26**, 404–421.
- GRANDISON, S., VANDEN-BROECK, J.-M., PAPAGEORGIU, D.T., MILOH, T. & SPIVAK, B. 2007 Axisymmetric waves in electrohydrodynamic flows. *J. Engng Maths* **62**, 133–148.
- HUNT, M.J., VANDEN-BROECK, J.-M., PAPAGEORGIU, D.T. & PĂRĂU, E.I. 2017 Benjamin–Ono Kadomtsev–Petviashvili’s models in interfacial electro-hydrodynamics. *Eur. J. Mech. (B/Fluids)* **65**, 459–463.
- JOSHI, A., RADHAKRISHNA, M.C. & RUDRAIAH, N. 2010 Rayleigh–Taylor instability in dielectric fluids. *Phys. Fluids* **22**, 064102.
- KOCHURIN, E.A. & ZUBAREV, N.M. 2018 Gravity-capillary waves on the free surface of a liquid dielectric in a tangential electric field. *IEEE Trans. Dielec. Elec. Insul.* **25**, 1723–1730.
- LAGET, O. & DIAS, F. 1997 Numerical computation of capillary-gravity interfacial solitary waves. *J. Fluid Mech.* **349**, 221–251.
- MELCHER, J.R. 1963 *Field-Coupled Surface Waves*. MIT Press.
- MELCHER, J.R. & SCHWARZ, W.J. 1968 Interfacial relaxation over stability in a tangential electric field. *Phys. Fluids* **11**, 2604.
- MELCHER, J.R. & TAYLOR, G.I. 1969 Electrohydrodynamics: a review of the role of interfacial shear stresses. *Annu. Rev. Fluid Mech.* **1**, 111–146.
- MILEWSKI, P.A., VANDEN-BROECK, J.-M. & WANG, Z. 2011 Hydroelastic solitary waves in deep water. *J. Fluid Mech.* **679**, 628–640.
- PAPAGEORGIU, D.T. 2019 Film flows in the presence of electric fields. *Annu. Rev. Fluid Mech.* **51**, 155–187.
- PAPAGEORGIU, D.T., PETROPOULOS, P.G. & VANDEN-BROECK, J.-M. 2005 Gravity capillary waves in fluid layers under normal electric fields. *Phys. Rev. E* **72** (5), 051601.
- PAPAGEORGIU, D.T. & VANDEN-BROECK, J.-M. 2004a Large-amplitude capillary waves in electrified fluid sheets. *J. Fluid Mech.* **508**, 71–88.
- PAPAGEORGIU, D.T. & VANDEN-BROECK, J.-M. 2004b Antisymmetric capillary waves in electrified fluid sheets. *Eur. J. Appl. Maths* **15**, 609–623.
- PAPAGEORGIU, D.T. & VANDEN-BROECK, J.-M. 2007 Numerical and analytical studies of non-linear gravity-capillary waves in fluid layers under normal electric fields. *IMA J. Appl. Maths* **72**, 832–653.
- PETVIASHVILI, V.I. 1976 Equation of an extraordinary soliton. *Sov. J. Plasma Phys.* **2**, 257–258.
- SCHÄFFER, E., THURN-ALBRECHT, T., RUSSELL, T.P. & STEINER, U. 2000 Electrically induced structure formation and pattern transfer. *Nature* **403**, 874–877.
- TAYLOR, G.I. 1964 Disintegration of water droplets in an electric field. *Proc. R. Soc. Lond. A* **280**, 383–397.
- TAYLOR, G.I. & MCEWAN, A.D. 1965 The stability of a horizontal fluid interface in a vertical electric field. *J. Fluid Mech.* **22**, 1–15.
- TILLEY, B.S., PETROPOULOS, P.G. & PAPAGEORGIU, D.T. 2001 Dynamics and rupture of planar electrified liquid sheet. *Phys. Fluids* **13**, 3547–3563.
- TURNER, R.E.L. & VANDEN-BROECK, J.-M. 1988 Broadening of interfacial solitary waves. *Phys. Fluids* **31** (9), 2486–2490.
- WANG, Z. 2017 Modelling nonlinear electrohydrodynamic surface waves over three-dimensional conducting fluids. *Proc. R. Soc. Lond. A* **473**, 20160817.
- YANG, Q., LI, B.Q., ZHAO, Z., SHAO, J. & XU, F. 2016 Numerical analysis of the Rayleigh–Taylor instability in an electric field. *J. Fluid Mech.* **792**, 397–434.



*Interfacial electrohydrodynamic solitary waves*

- ZAKHAROV, V.E. 1968 Stability of periodic waves of finite amplitude on the surface of a deep fluid. *J. Appl. Mech. Tech. Phys.* **2**, 190–194.
- ZUBAREV, N.M. 2004 Nonlinear waves on the surface of a dielectric liquid in a strong tangential electric field. *Phys. Lett. A* **333**, 284–288.